PCM THERMAL CONTROL OF NICKEL-HYDROGEN BATTERIES

Dr. Timothy R. Knowles

Energy Science Laboratories, Inc.
6888 Nancy Ridge Drive
San Diego, CA 92121-2232

June 1993

Final Report

19960215 040

PHILLIPS LABORATORY
Space and Missiles Technology Directorate
AIR FORCE MATERIEL COMMAND
KIRTLAND AIR FORCE BASE, NM 87117-5776

UNCLASSIFIED

AD NUMBER

AD-B207 046

NEW LIMITATION CHANGE

TO

DISTRIBUTION STATEMENT A -
Approved for public release; Distri-
bution unlimited.

Limitation Code: 1

FROM

DISTRIBUTION STATEMENT   -

Limitation Code:

AUTHORITY

Janet E. Mosher, Phillips Lab/CA, Kirtland AFB, N.M.

THIS PAGE IS UNCLASSIFIED

PL-TR-93-1075

This final report was prepared by Energy Science Laboratoreis, Inc., San Diego, CA Contract F29601-92-C-0065 Job Order, 9991SB1R, with Phillips Laboratory, Kirtland Air Force Base, New Mexico. The Laboratory Project Officer-in-Charge was Larry Crawford (VTPT).
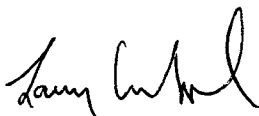
When Government drawings, specifications, or other data are used for any purpose other than in connection with a definitely Government-related procurement, the United States Government incurs no responsibility or any obligation whatsoever. The fact that the Government may have formulated or in any way supplied the said drawings, specifications, or other data, is not to be regarded by implication, or otherwise in any manner construed, as licensing the holder, or any other person or corporation; or as conveying any rights or permission to manufacture, use, or sell any patented invention that may in any way be related thereto.

This report has been authored by a contractor of the United States Government. Accordingly, the United States Government retains a nonexclusive royalty-free license to publish or reproduce the material contained herein, or allow others to do so, for the United States Government purposes.

This report contains proprietary information and shall not be either released outside the government, or used, duplicated or disclosed in whole or in part for manufacture or procurement, without the written permission of the contractor. This legend shall be marked on any reproduction hereof in whole or in part.

If your address has changed, if you wish to be removed from the mailing list, or if your organization no longer employs the addressee, please notify PL/VTPT, 3550 Aberdeen Ave SE, Kirtland AFB, NM 87117-5776 to help maintain a current mailing list.

This report has been reviewed and is approved for publication.

LARRY CRAWFORD
Project Officer

FOR THE COMMANDER

DAVID KRISTENSEN, Lt Col, USAF
Chief, Space Power and
Thermal Management Division

HENRY L. PUGH, JR., Col, USAF
Director of Space and Missiles Technology

DO NOT RETURN COPIES OF THIS REPORT UNLESS CONTRACTUAL OBLIGATIONS OR NOTICE ON A SPECIFIC DOCUMENT REQUIRES THAT IT BE RETURNED.

DRAFT SF 298

1. Report Date (dd-mm-yy) June 1993	2. Report Type Final	3. Dates covered (from... to) 5/92 to 11/92
4. Title & subtitle PCM Thermal Control of Nickel-Hydrogen Batteries		5a. Contract or Grant # F29601-92-C-0065
		5b. Program Element # 62601F
6. Author(s) Dr. Timothy R. Knowles		5c. Project # 9991
		5d. Task # SB
		5e. Work Unit # 1R
7. Performing Organization Name & Address Energy Science Laboratories, Inc. 6888 Nancy Ridge Drive San Diego, CA 92121-2232		8. Performing Organization Report #
9. Sponsoring/Monitoring Agency Name & Address Phillips Laboratory 3550 Aberdeen Ave SE Albuquerque, NM 87117-5776		10. Monitor Acronym
		11. Monitor Report # PL-TR-93-1075

12. Distribution/Availability Statement   Distribution authorized to DoD components only; Proprietary Information; June 1993; Other requests for this document shall be referred to AFMC/STI.

13. Supplementary Notes

14. Abstract

The cycle life of Ni-H_2 batteries is sensitive to temperature control and satellite batteries generally have dedicated radiator and heater subsystems. Because batteries are often used in high-rate transient modes, passive thermal control with latent heat materials can be effective. This project investigates battery thermal control with phase-change materials (PCMs) that absorb heat dissipated during high rate discharge and release it slowly thereafter, all occurring within a small temperature range. The intrinsic heat capacity of Ni-H2 batteries is rather low, and common PCMs enable the effective battery heat capacity to be increased by 300% in the temperature range from -5°C to +5°C with a mere 10% weight penalty. The benefits to cycle life, reduction in space radiator weight and size, and savings in battery heater power outweigh the PCM cost for a variety of applications. Illustrative cases are modeled for both high earth and low earth orbits.

15. Subject Terms

Nickel-Hydrogen Batteries, Phase-Change Materials, Satellite Batteries, Battery Thermal Control

Security Classification of			19. Limitation of Abstract	20. # of Pages	21. Responsible Person (Name and Telephone #)
16. Report Unclassified	17. Abstract Unclassified	18. This Page Unclassified	Limited	60	Larry Crawford (505) 846-0477

GOVERNMENT PURPOSE LICENSE RIGHTS
(SBIR PROGRAM)

Contract Number: F29601-92-C-0065
Contractor: Energy Science Laboratories, Inc.

For a period of two (2) years after delivery and acceptance of the last deliverable item under the above contract, this technical data shall be subject to the restrictions contained in the definition of "Limited Rights" in DFARS clause at 252.227-7013. After the two-year period, the data shall be subject to the restrictions contained in the definition of "Government Purpose License Rights" in DFARS clause at 252.227-7013. The Government assumes no liability for unauthorized use or disclosure by others. This legend shall be included on any reproduction thereof and shall be honored only as long as the data continues to meet the definition on Government purpose license rights.

TABLE OF CONTENTS

LIST OF FIGURES & TABLES

NOMENCLATURE

Abbreviations:

BOL	beginning of life
CCHP	constant conductance heat pipe
CPV	common pressure vessel
DOD	depth of discharge
EOL	end of life
ESLI	Energy Science Laboratories, Inc.
Na-S	sodium sulfur
Ni-H$_2$	nickel hydrogen
Ni-Cd	nickel cadmium
NiMH	nickel metal hydride
GEO	geosynchronous orbit
IPV	individual pressure vessel
LEO	low earth orbit
PCC	phase-change composite (PCM + conductive filler)
PCM	phase-change material
PV	photovoltaic
RC	thermal RC time constant
SBR	space based radar
SOC	state of charge
SSF	Space Station Freedom
TES	thermal energy storage
VCHP	variable conductance heat pipe

Symbols:

A	area [m^2]
c	volumetric heat capacity [J/K-m^3]
C	total heat capacity = c A L, [J/K]
d	fin thickness [m]
H	volumetric latent heat [J/m^3]
k	thermal conductivity [W/K-m]
ρ	density [kg/m^3]
P	power [W]
R	thermal resistance = L /(A k), [K/W]
τ	thermal time constant [s]
ΔT	temperature difference [K]
T	temperature [K]
ϕ	volume fraction of M component
z	depth of melted layer [m]

1   PROJECT SUMMARY

Purpose - Thermal control is a design driver for space applications of nickel-hydrogen (Ni-H_2) battery systems, because excessive temperatures shorten battery cycle life. Compared with the nickel-cadmium (Ni-Cd) batteries they are replacing, the Ni-H_2 batteries require lower operating temperatures but they generate higher heat loads. The space radiators that provide the cooling in satellites are generally sized to avoid damaging high temperatures during high-rate battery discharge. However, at other orbital phases when battery heat dissipation is low, the radiators cooling is excessive, and battery heaters are required to avoid damage by freezing.

This project considers increasing the effective heat capacity of the battery to reduce the heating requirements and downsize the radiators toward the orbital average load. In principle, doubling the effective battery heat capacity in the range from -5°C to +5°C can reduce transients by 50% but increases the battery mass by only 3%, assuming water is used through its phase change at 0°C. In practice, the reliability of the encapsulation and heat transfer are problematical. We consider innovative phase-change composite (PCC) design using conductive carbon fiber wick structures that perform well and appear to enable compact, reliable design.

Work done - Manufacturers and users were surveyed to identify candidate battery applications for various orbital missions. Preliminary analysis was performed to determine the range of thermal control behavior and the optimum phase-change material (PCM) quantity. A simple two-node system model describing the battery + PCM and the radiator was developed and used to assess the benefits of thermal energy storage in existing low earth orbit (LEO) and geosynchronous orbit (GEO) battery systems. The model agrees well with existing battery thermal data.

Designs were investigated having low weight, high overall thermal conductance, and capillary control of void distribution to relieve expansion stress. Figure 1 illustrates the design options considered. A series of composite storage test articles were fabricated with carbon fiber conductors and both organic and water PCMs. The test articles were thermally cycled through the phase transition. A full-scale illustrative composite sleeve structure for use with a Ni-H_2 cell was fabricated.

Results - Analysis shows that PCCs offer significant improvements in battery temperature control and significant weight savings in terms of reduced space radiator and heater power requirements. Benefits are strongest for high rate discharge applications such as GEO and LEO communications satellites, and satellites using surge battery power. Exterior sleeve designs are recommended for independent pressure vessels, and interior plate designs are recommended for common pressure vessel designs. Overall, the PCCs promise improved transient temperature control, improved temperature uniformity across the battery, reduced thermal control system weight, reduced radiator area, reduced solar array area, reduced heater power.

A significant achievement is the control of the volume change and expansion stress in freezing ice through the use of carbon fiber wick structures.

PCC = PCM + fins

— metal or composite liner

— radial fiber fins

— helical foil fins

— longitudinal foil fins
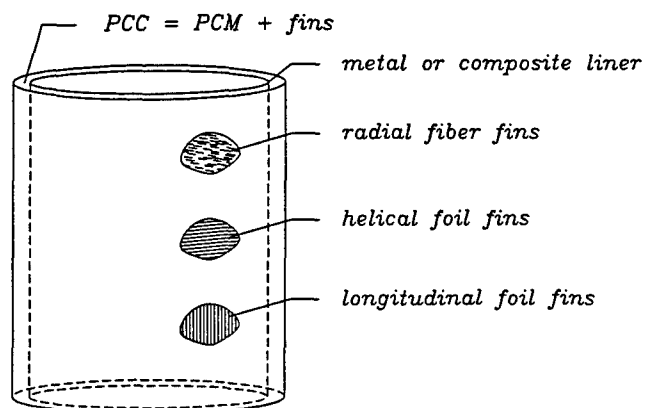
Figure 1   PCC conductivity structure design options.

Benefits -
- tighter battery temperature control
- longer cycle life
- higher battery efficiency
- reduced battery heater power
- reduced weight and size of the battery thermal control system

Applications - Satellite battery systems in both small and large satellites for both low and high earth orbits. Battery thermal control in surge power systems such as space based radar. Thermal control of high temperature sodium-sulfur batteries for satellite and electric vehicle applications.

Generic thermal energy storage applications exist for the innovative encapsulated water composite system having high thermal conductance and low expansion stress.

2 INTRODUCTION

2.1 Spacecraft Battery Systems

Ni-H$_2$ battery temperature sensitivity - Nickel-hydrogen batteries are generally displacing Ni-Cd batteries in space systems because of their higher capacity, higher power density, and longer cycle life. The associated thermal control problems are escalating, however, because these batteries operate at lower temperatures than Ni-Cd batteries, and they dissipate greater heat. Battery reliability is strongly dependent on good thermal control, and battery failures have been attributed to

- excessively high temperatures that dramatically shorten cycle life
- excessively low temperatures that freeze electrolyte and rupture separators
- intercell temperature gradients that cause imbalance in charge efficiency and discharge current
- intracell temperature gradients that cause electrolyte to migrate within the cell and reduce charge balance and cell efficiency

Ni-H$_2$ battery heat capacity - Nickel-hydrogen batteries have a large metal fraction and their specific heat is approximately 1 J/g-K. In comparison, PCMs have high heat capacity. For example, the fusion enthalpy (latent heat) of water is 334 J/g. The enthalpy change of water between -5°C and +5°C is 375 J/g, so that the effective heat capacity averaged over this temperature range is fully 37 times greater than that of Ni-H$_2$ battery. Incorporation of a PCC based on water can increase the effective heat capacity of a battery over that temperature range by 100%, while adding merely 3% weight.

Some battery systems are designed with large capacity margins. For example the Hubble Space Telescope Ni-H$_2$ batteries are sized to operate at less than 8% depth of discharge (DOD). Low DOD extends battery cycle life for a variety of reasons. The thermal control of this battery is extremely good, partly because of the huge heat capacity. Note that if a battery half that size were operated at twice the rate of discharge, then merely 1.5% of that weight (total weight = 51.5% of original battery weight) would be required to achieve the same heat capacity.

Cell thermal runaway - In some circumstances a battery cell will run warm as a result of some fabrication irregularity or a local environmental reason. This situation tends to become aggravated as follows:

CHARGE - The warmer cell will have a lower charge efficiency and therefore higher heat generation, which increases its temperature further. Higher temperature favors the competing reaction of water electrolysis. The recombination occurs on the platinum catalysts provided for this purpose, which also results in heat generation.

DISCHARGE - The warmer cell has higher discharge voltage and lower electrolyte resistance. It therefore takes a larger fraction of the load and discharges more rapidly.

A warm cell in a battery tends to discharge more deeply and to recharge less efficiently. Both of these effects reduce the cycle life of that cell and consequently of the battery in which it is a part. In usual Ni-H$_2$ battery configurations, the first failure of a cell means failure of the battery.

Cold-bias design - Thermal control of space batteries for geosynchronous communication satellites generally follows a "cold-bias" design, in which an excess cooling capacity is provided together with extra heating capacity. The combination allows good control, at the cost of a somewhat larger radiator for cooling and a larger allocation from the satellite photovoltaic power system. Space batteries need heating during low rate charge, when photovoltaic power is in demand. This design is chosen by necessity to provide cooling for the high dissipation modes of operation where the cooling system may see a multiple of the average load for several to tens of minutes.

An alternative design that is potentially smaller, lighter and consumes less power is to provide additional heat capacity to the battery. The higher heat capacity can accommodate the heat during high rate dissipation, so that a smaller radiator can be used, and then permit the dissipating to occur over a longer time scale. Another important benefit is that by releasing the heat slowly through the smaller radiator, the need for battery heater power during the charge phase is reduced.

2.2   Passive Thermal Control with PCCs

High heat capacity acts like a low-pass filter in a thermal circuit. Placed between a fluctuating heat source and a radiative heat sink such as common in satellites, thermal energy storage (TES) reduces the fluctuations in the heat load delivered to the radiator, allowing it to be downsized to the time-averaged load. The relevant time constant for the variations is given by $\tau = RC$, where C is the total heat capacity and R is the total thermal resistance (larger for smaller radiators). It is desired to have a large value of τ, on the order of the orbital time. The situation is illustrated schematically in Figure 2. The large latent heat of transition contributes to the effective volumetric heat capacity of the PCM near its phase transition temperature:

$$c_{eff} = c + \frac{H}{\Delta T}$$

where c is the sensible heat capacity, H is the latent heat, and ΔT is the temperature range over which the PCM is used (including the transition temperature). Because the Ni-H$_2$ battery is held to a small temperature range ~ 10 K, the latent heat contribution to the effective heat capacity can be large. There are numerous organic and inorganic candidate PCMs that offer effective heat capacities 20-50 times greater by weight and roughly 10 times smaller by volume than the intrinsic heat capacity of Ni-H$_2$ batteries.

PCC TES AVERAGES HEAT LOAD

Phase front moves when input power changes
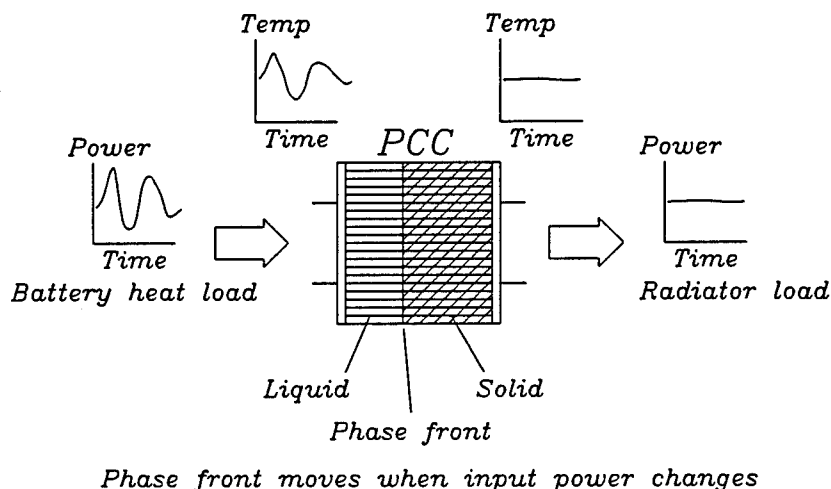
Figure 2   PCC thermal storage averages the heat load delivered to the radiator, allowing it to be sized for the smaller average load.

Heat capacity is useful only if it is adequately coupled to the source of heat. ESLI has been developing PCCs that consist of high thermal conductivity (high-k) filler material that is finely dispersed in a high heat capacity (high-c) phase-change matrix. Aluminum foil or graphite fibers are generally used for the high-k component and low density organic and inorganic materials are used for the high-c component. Such PCCs have been shown [Knowles, 1986] to overcome the two major problems associated with using PCMs for heat storage:

- poor thermal conductivity limiting the rate of heat absorption or release, and
- stress resulting from expansion during phase change

The reasons PCC design overcomes these problems is discussed in more detail in Section 4.2.

2.3   Phase 1 Technical Objectives

The technical objectives of this Phase 1 SBIR project are:

Task 1.   Survey NiH2 space battery systems and identify candidate applications.
Task 2.   Select materials for study.
Task 3.   Model thermal behavior and quantify net spacecraft system benefits.
Task 4.   Fabricate and cycle-test PCC coupons.
Task 5.   Develop draft design for Phase 2 prototype.

5

3   BATTERY THERMAL CONTROL

3.1   Cell Heat Dissipation

<u>Ni-H$_2$ cell reactions</u> - During discharge of the Ni-H$_2$ cell, nickelic oxide at the positive
electrode is reduced to nickelous oxide (as in the Ni-Cd battery) and hydrogen is oxidized to water at
the negative electrode. The half cell processes (forward reactions for discharge; reverse reactions for
charge) are:

$$anode\ reaction: \quad NiOOH + H_2O + e^- \quad \rightleftarrows \quad Ni(OH)_2 + OH^- \tag{2}$$

$$cathode\ reaction: \quad 1/2\,H_2 + OH^- \quad \rightleftarrows \quad H_2O + e^- \tag{3}$$

$$net\ reaction: \quad NiOOH + 1/2\,H_2 \quad \rightleftarrows \quad Ni(OH)_2 \tag{4}$$
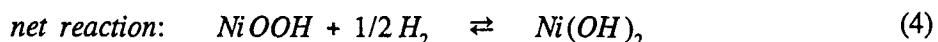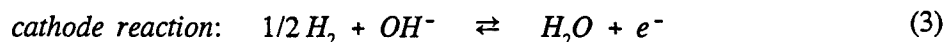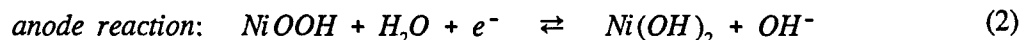
The negative anode is oxidized to supply electrons to the electrical circuit and the positive cathode is
reduced. The Ni-H$_2$ cell has intrinsic overcharge protection, which is a benefit compared with Ni-Cd
cells. During overcharge of the Ni-H$_2$ cell, the O$_2$ evolved at the anode recombines
electrocatalytically with H$_2$ evolved at the platinum cathode, dissipating heat and forming water, but
not causing a net pressure buildup. During cell reversal, pressure does not increase because H$_2$ is
simultaneously evolved at the anode and consumed at the cathode.

<u>Heat generation processes</u> - The coulombic efficiency of the battery and its heat dissipation
depend on the cell temperature, the charge or discharge rate and state of charge (SOC). There are
several models in use to describe the heat dissipation.

The power dissipation may be expressed in terms of the instantaneous cell potential and
current. The part of the current that goes to oxygen evolution during charge is singled out. It is
assumed that the oxygen evolution current is a function of the corrected cell potential (V-iR), is
independent of SOC, and immediately recombines with hydrogen to generate heat, so that

$$charge: \quad P = i_c\,(V - V_0) + i_e\,V \tag{5}$$

$$discharge: \quad P = i_d\,(V_0 - V) \tag{6}$$

where V is the instantaneous cell potential, V_0 is the thermal neutral potential, and i_e is the oxygen
evolution current.

Kerr [Kerr, 1986] expresses the heat dissipation as follows

$$\text{charge:} \qquad P = i\ (V + \frac{\Delta H}{2F}\ \eta\ ) + V\ \frac{\partial P_g}{\partial t} \tag{7}$$

where η is charge efficiency, ΔH is the molar enthalpy change, F is the Faraday number, and P_g is the gas pressure. A similar expression is used for discharge except that η is assumed to be unity.

Scott [Scott, 1983] expresses the heat dissipation as

$$\text{charge, discharge:} \qquad P = i\ (\eta\ V_0 - V\ ) \tag{8}$$

where η is the instantaneous coulombic efficiency. For discharge $\eta = 1$, and for charge the value used is derived from instantaneous pressure data. The formula does not agree well with observations for charging, presumably because of poor understanding of the oxygen evolution current.

In general, the cell current is composed of three contributions: $I = I_{charge} + I_{hydrolysis} + I_{Ohmic}$. Exactly how these components depend on the total current, the temperature and the SOC is not well understood. In summary, heat dissipation is best estimated from *observed* values of the current and voltage, according to

$$P = i\ (V_0 - V\ ) \tag{9}$$

where V_0 is the thermal neutral voltage = 1.52 V for the Ni-H$_2$ cell.

Interior cell temperatures - Ryu [Ryu, 1991] reports modeling of the cell interior temperatures as a function of the current and state of charge. Their initial results, obtained with the assumption that the pressure vessel wall temperature is isothermal and constant, indicate that the nickel electrode is 20°C hotter than the wall, and the maximum temperature is achieved at end of charge.

3.2   Cell Heat Capacity

Although batteries are usually heavy, frequently hundreds of kilograms, the total heat capacity is not high when compared with the heat dissipation. Nickel-hydrogen batteries have low specific heat $c \approx 1$ J/g-K, characteristic of the metals that comprise the majority of the mass of the battery. Phase-change materials have high effective heat capacity when the latent heat contribution is included. For example, the fusion enthalpy (latent heat) of water is 334 J/g. Integrated over the temperature range from -5°C to 5°C, the heat capacity of water is 37 times greater than that of an equivalent weight of Ni-H$_2$ battery. Using water as the PCM, the heat capacity of a battery can be increased 100% while adding only 3% weight.

3.3   Potential PCM Applications

3.3.1   LEO Missions

Low earth orbit missions are characterized by a discharge cycle per 90-minute orbit, making ~6000 cycles per year. The heat dissipation peaks for approximately 15 minutes per cycle. Certain LEO applications, such as radar and mobile telephone satellites, can have high rate discharge for short time times. Specific missions are discussed below.

Space Station - The Space Station Freedom (SSF) batteries are large (100 kW) and located in the external vacuum environment. They are however coupled to the coolant bus, and thermal control is not considered a problem. There is concern with the temperature uniformity along a cell and among the different cells in the batteries. Phase change composites could have a benefit in this regard.

Space Based Radar - Only limited information is available on space based radar thermal control. Surge or burst modes are mentioned [Metcalfe, 1993] where tens of kilowatts of battery power are required. The radar pulse time characteristic is 30 ms on, 30 ms off. The duration of the pulse train depends on the application, and durations from 1 to 15 minutes are anticipated. Because the duration of the high power mode is short, PCC thermal control is potentially beneficial in this application.

Iridium, Global Star, etc - The new satellite mobile telephone systems under development call for constellations of LEO satellites. A thermal problem unique to this system is that high traffic centers (major cities) will load the nearest satellite with high transmission activity for a duration of several minutes until the satellite passes out of range. This high power demand will be fed primarily by the battery and is likely to occur during daytime when solar thermal loading is maximum and the cooling system is least effective. Because the power level is high for a limited duration of several minutes, this application appears to be a good one for PCM thermal control.

ERS-1 Satellite - The ERS-1 Satellite is a European Space Agency radar satellite using Synthetic Aperture Radar (SAR) to image sites around the world. By the end of 1992 it had transmitted ~300,000 images, each of which takes 15 seconds to generate. The SAR is used not more than 7 minutes per orbit, because of its high energy consumption. Such high rate discharge is very likely to verge on thermal control problems in its $Ni-H_2$ batteries. Because the duty cycle is only 7 minutes /95 minutes = 7.4%, this system and others like it may be good LEO applications for PCCs. The benefit of PCM thermal control would be improved reliability as a result of better temperature control and potentially greater on-time duration.

3.3.2 GEO Missions

GEO communications satellites - The GEO missions experience two eclipse seasons per year near the equinoxes. The batteries experience a total of 88 cycles in which the deepest discharges occur at the middle of the season when the eclipse duration is longest. The longest discharge period is ~72 minutes. There is a low power dissipation as a result of battery trickle charge for most of the rest of the orbit.

The GEO communications satellites tend to have a thermal control system that is cold-biased with a radiator sized larger than the average power, and with heaters that are used to avoid excessively low temperatures. Under the best of circumstances, the radiator is sized only slightly above the average power dissipation so that little heater power is required, and the temperature excursions are not excessive.

The potential benefits of PCMs control in GEO satellites are:
- reduce temperature excursions during discharge, improving battery reliability
- smaller radiator and battery area
- smaller demand for heater power, reducing size of photovoltaic (PV) array

In some cases the latter benefits can not be enjoyed because the minimum radiator and heater sizes are determined by other quirks of the overall design. For example, some INTELSATs have *side* panels that carry the PV arrays. The north and south panels each have a battery that experiences environmental extremes from season to season. For example, at each solstice one of the two batteries is out of the sun and requires heater power. In these satellites the radiator is sized for trickle charge in sun at end of life (EOL) when solar absorptivity is higher, and the heater is sized for the equinox charging at beginning of life (BOL), typically requiring 75 W of the 5 kW PV power system. The PV system is sized for solstice when power is at a premium because the PV system must provide normal load requirements, trickle charge, battery heating; moreover the PV panel is inclined 23° at this phase of the orbit. Thus, the radiator size and heater power are determined independently of battery transients. What happens during transients is more or less just accepted because there is a high cost of providing any other thermal control options. For example, increasing battery radiator area to reduce temperature excursion increases the heater power required at other times.

3.3.3 Retrofitting Ni-H$_2$ Batteries

Retrofitting existing satellite systems with Ni-H$_2$ batteries in place of original Ni-Cd batteries can lead to increased heat dissipation. That effect, together with the lower operating temperature requirement of Ni-H$_2$ batteries, can lead to a requirement for larger space radiators to meet peak cooling loads. The use of PCC can avoid such radiator changes through the load-leveling effect of higher heat capacity.

9

3.3.4 Other Space Batteries

Mars Lander - The NASA Mars Environmental Survey program involves small mars lander craft that will encounter a variety of thermal conditions where PCC thermal control may be useful. The problem is the cold (-90°C) martian night that threatens to freeze the batteries. One design option is to employ a PCC inside a highly insulated package containing the batteries. During daytime PV power may be used to electrically heat the PCC to provide adequate heat to survive the slow heat leak during the night.

McDonnell-Douglas Modular Power Systems - A potential application of PCC is in the Transporter Energy Storage System (TESS) on the SSF Mobile Transporter. This transporter hauls gear along the trusses of the SSF and it has a manipulator arm. Thermal control considerations currently limit the duration of activity for the Transporter, and thermal energy storage with PCC may enable longer operations.

EVA Manpack Battery - PCC may be useful for extravehicular activity battery manpacks. Prior studies concluded that aluminum foam conductivity structure with metal encapsulation weighed so much that the benefit of the PCM was greatly discounted. The risk of leakage was also significant. Present manpack batteries use new "double-D" lithium cells that have higher power and higher heat dissipation. There is a growing concern that the maximum permissible temperature of 72°C will be exceeded. This could be an application for PCC thermal control based on the lightweight carbon fiber wick design developed in this project.

Common Pressure Vessels - The Common Pressure Vessel (CPV) designs uses one encapsulating vessel for a large number of cells. There are benefits in terms of battery compactness and weight savings. Thermal problems with the CPV design arise from the longer conduction path for heat dissipation from the interior and the smaller total surface area of the battery, compared with the independent pressure vessel design. An existing design (Johnson Controls) for a 22-cell 50-Ahr capacity battery, requires a number of metal plates 0.5 mm thick and 25 cm in diameter that conduct heat to the vessel wall.

An alternative thermal control means is to use PCC *inside* the CPV, where it may be stored beneficially for the next charge cycle. The scheme avoids the need to transfer as much heat through the vessel surface. Especially for high-rate discharge applications this would be an attractive option. The weight of the PCC plates can be discounted by the weight saved on the usual conductive plates. The concept is illustrated in Figure 3.

Kim [1992] cites relevant CPV thermal parameters and emphasizes that a gradient in excess of 8.4 K can cause electrolyte redistribution that is damaging to the cells. The authors accordingly have calculated the thickness required for copper conducting plates required to meet this gradient constraint, and they find 15-mil copper is required. The weight fraction of the copper fins is 6% of the entire battery.

COMMON PRESSURE VESSEL (eg 22 cells)

Ni-H2 cells in polybags

metal plate heat conductor

vessel wall
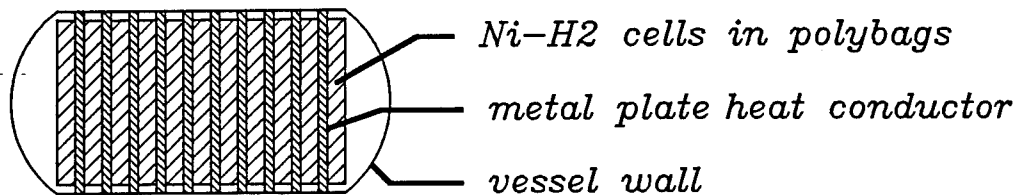
PCC OPTION: Replace metal plate with high-c plate.

PCC core

* high capacity
* low weight
* improved Temp control
* reduced GEO heating requirement
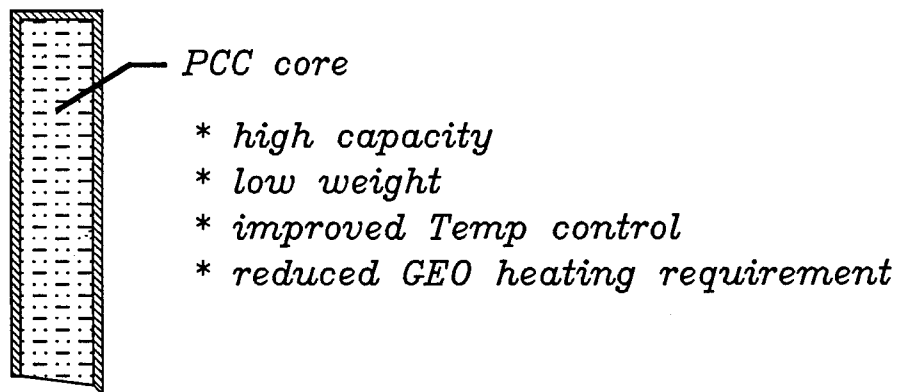
Figure 3   Concept for PCC plates in CPV thermal control packaging.

11

3.3.5 Electric Vehicle Batteries

Na-S Vehicle Batteries - For high efficiency and long cycle life, Na-S batteries must be operated within a narrow band of elevated temperatures T = 350±15°C. To reduce steady heat losses, the batteries are usually well insulated. For electric vehicles the goal is a heat leak of 0.1 kW per vehicle. Under driving conditions, however, the batteries generate 5-10 kW of internal waste heat, which can overheat the cells in 15 minutes. To meet the design goal of 60-minute high-rate operation, battery temperature control is required. Active temperature control using a pumped coolant has the disadvantage that it must penetrate the insulation, unavoidably degrading it. Passive temperature control using a material having high heat capacity placed within the insulated battery is another option illustrated in Figure 4.

PCM thermal storage - Phase change materials can store heat in comparatively small volumes of material.   For example, storing 10 kWh of heat at T = 350±15°C in Na-S batteries requires approximately 1500 kg of cells, whereas water requires only 80 kg (88 liter) to store 10 kWh of heat at T = 0±15°C. This PCM is therefore ≈ 20 times lighter than Na-S cells in accommodating heat. Generally the effectiveness of PCMs, compared with ordinary heat storage, increases with increasing temperature. For example, 10 kWh of heat may be stored in only 32 kg (15 liter) of lithium fluoride at T = 848±15°C).

Candidate PCMs - The temperature range 300-400°C is one where very little thermal energy storage experience has been gathered. In a preliminary survey, ESLI identified ~3000 PCMs in this range, but very few have been thermally characterized. Selected cases where the data are known are shown in the Table IV. To store 10 kWh of heat, the lowest weight found in the temperature range of interest is 130 kg, and the lowest volume found is 45 L. The materials sited are not particulary attractive options. Not represented are the polymeric materials with low average atomic weights and
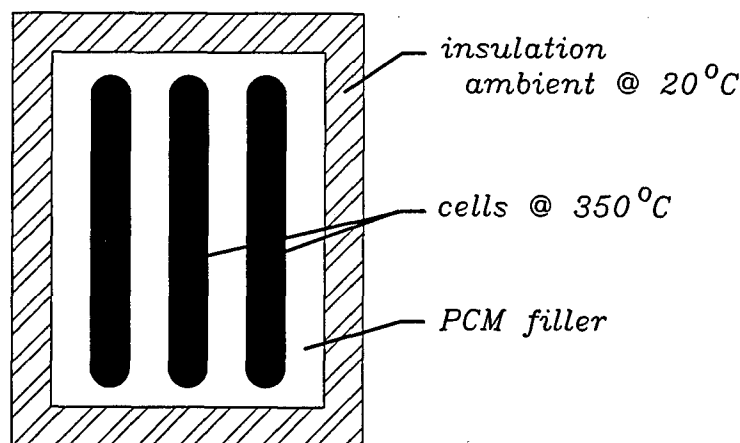
Figure 4   Passive thermal control using PCM inside the battery.

strong crystallinity. Such materials must be custom synthesized, and sufficient need apparently has not arisen before. Polymers based on silicon (Si-, Si-O, Si-N) are promising for their stability, compatibility, density and potentially high latent heats. The compounds will require molecular tailoring to favor crystallinity in the solid phase. A reasonable goal is shown in the last row of Table I. Once identified, the cost of polymer synthesis may be similar to that for commercial synthetic lubricants.

Table I Phase change material candidates for storing 10 kWh heat within $\Delta T = 30°C$ at $350°C$.

Material		Weight (kg)	Volume (Liter)
Sodium-sulfur cells		1500	600
H_2O, Water	(PCM @ 0°C)	80	88
LiF	(PCM @ 850°C)	32	15
Zn-Al	(PCM @ 382°C)	320	45
KN_3	(PCM @ 346°C)	130	135. (est.)
Zn-Al/KN_3	(PCM @ 346-382°C)	225	90
New Polymer	(PCM @ 350°C)	< 50?	< 50?

4   PHASE CHANGE COMPOSITE DEVELOPMENT

The PCC is a composite of high-c PCM and high-k filler that serves both to increase thermal conductance and control the location of the liquid PCM by wicking action. This section describes the selection of component materials and the fabrication and testing of PCC thermal energy storage devices.

4.1   Materials Selection

4.1.1   PCM Candidates

Numerous PCMs - A search for PCMs having suitable characteristics was conducted. The On-Line Beilstein Compendium lists more than 10,000 PCMs having melting points in the temperature range from -20°C to 10°C. The Aldrich Chemical company lists approximately 500 such materials for sale. Of the latter materials, only a small fraction have latent heat data available. Using thermal data [Landolt-Bornstein, 1961] we selected candidate PCMs that appeared to have high latent heat and are otherwise candidates based on price or potential chemical compatibility with other materials. The resulting list of 54 materials is presented in Table II.

PCMs selected for testing - Two PCMs were selected for this effort: the normal paraffin n-tetradecane and water, whose properties are summarized in Tables III and IV. Paraffin PCMs have been used before [Gilmore, 1992] in spacecraft thermal control and are regarded as benign materials having good latent heat, stability and compatibility with common encapsulation materials. Tetradecane (#43 in Table V) is one that falls in this range (note that Aldrich incorrectly lists the melting point as -5°C).

Water is a candidate because it has very high latent heat and it is available in pure form at low cost. If paraffin is used in place of water, approximately 50% more PCM mass and 100% more PCM volume is required for the same latent heat. The two other materials with higher latent heats, hydrazine and hydrogen cyanide, are both ruled out because of their explosion and toxicity hazards, respectively. The outstanding problem with water that has kept it from being used in spacecraft PCM canisters is that it has a tremendous ability to rupture its encapsulation. To use water effectively, it is critical to manage the thermal expansion of this material.

A related PCM is heavy water (deuterium oxide) in which the hydrogen isotope D replaces one or both H atoms in the normal H_2O water molecule. It is a well established, but little known, fact that water/heavy water mixtures have melting points that can be adjusted precisely anywhere in the temperature range 0 - 3.8°C. Furthermore, the melting point remains very sharp and the latent heat is essentially not degraded by the mixing. Mixtures generally do not behave this way. For

14

Table II　　　PCMs with melting point between -17°C and +10°C

	chemical name	formula	melting point (°C)	latent heat (J/g)
1	o-dichlorobenzene	C6H4Cl2	-16.7	88
2	4,6-dimethylindan	C11H14	-16.7	88
3	2,2-dimethylpropane	C5H12	-16.6	45
4	arsenic trichloride	AsCl3	-16	56
5	quinoline	C9H7N	-15.6	84
6	benzyl alcohol	C7H8O	-15.2	83
7	benzyl methyl ketone	C9H10O	-15	
8	1-octanol	C8H18O	-15	
9	thiophenol	C6H6S	-14.9	104
10	1,1-dimethylazoethane	C8H18N2	-14.6	72
11	hydrogen cyanide	CHN	-13.4	311
12	ethylene glycol	C2h6O2	-13	146
13	n-dodecane	C12H26	-12	215
14	n-dodecane	C12H26	-9.6	215
15	tetraethyl glycol	C8H18O5	-9.4	
16	nitrogen tetraoxide	N2O4	-9.3	159
17	bromine	Br2	-8.25	66
18	cycloheptane	C7H14	-8.03	19
19	1,2,3,4-tetramethylbenzene	C10H14	-7.7	84
20	heptane acid	C7H14O2	-7.5	115
21	m-dibromobenzene	C6H4Br2	-6.9	56
22	aniline	C6H7N	-6.3	113
23	1,2,3,4-tetra methyl benzol	C10H14	-6.2	53
24	n-tridecane	C13H28	-6	155
25	arsenic trifluoride	AsF3	-5.9	79
26	bromotrichloromethane	CBrCl3	-5.7	13
27	n-butyric acid	C4H8O2	-5.7	126
28	5-nonanone	C9H18O	-3.9	175
29	caprone acid	C6H12O2	-3.6	130
30	chloronaphthalene	C10H7Cl	-2.5	79
31	bromonaphthalene	C10H7Br	-1.8	73
32	laurinsaeureaethylester	C14H28O2	-1.7	163
33	caprolactone	C6H12O2	-1.02	121
34	4,7-dimethylindan	C11H14	-0.5	92
35	hydrogen peroxide	H2O2	-0.43	367
36	hydrogen oxide (water)	H2O	0	333
37	1,1,4,6-tetramethylindan	C13H18	0.36	90
38	phosphoryl chloride	Cl3OP	1	86
39	hydrazine	H4N2	1.4	394
40	o-dibromobenzene	C6H4Br2	1.8	53
41	4 methoxybenzaldehyde	C8H8O2	2.5	
42	deuterium oxide	D2O	3.76	314
43	n-tetradecane	C14H30	5.5	228
44	benzene	C6H6	5.53	127
45	nitrobenzene	C6H3NO2	5.7	94
46	cyclohexane	C6H12	6.6	32
47	1,4-dimethylnaphthalene	C12H12	6.8	102
48	1-decanol	C10H22O	6.88	
49	tetralone	C10H10O	7	
50	formic acid	CH2O2	7.8	247
51	m-bromoiodobenzene	C6H4BrI	9.3	43
52	2-chlorophenol	C6H3ClO	9.8	97
53	1,2-dibromomethane	C2H4Br2	9.93	58
54	n-pentadecane	C15H32	10	205

example, sharp melting points are usually found only at specific compositions such as eutectic points. This behavior is traceable to the anomalous proton mobility in water, which causes the mixture to behave like a pure substance of composition $D_xH_{2-x}O$. Tritium is radioactive and therefore not considered further for this application.

Table III   Relevant mechanical properties of water and ice

WATER		0°C		50°C	100°C
		solid	liquid	liquid	liquid
density	(g/cm³)	0.917	1.000	0.988	0.958
specific volume	(cm³/g)	1.091	1.000	1.012	1.044
compressibility	(MPa⁻¹)	5.01×10^{-4}	5.04×10^{-4}	4.40×10^{-4}	4.80×10^{-4}

NOTE: The melting point of water at pressure 100 MPa is -9.0°C.

Table IV   PCMs selected for Phase 1 testing.

n-TETRADECANE ($C_{14}H_{30}$)
- benign paraffin that wets carbon fiber
- MP = 5.5°C; BP = 254°C; FP = 99°C; MW = 198.4
- H = 227 J/g; c = 2.21 J/g-K; ρ = 0.763 g/cm³ @ 20°C

WATER (H_2O)
- high latent heat, but large thermal stress
- MP = 0°C (range); BP = 100°C;
- H = 334 J/g; c = 4.19 J/g-K; ρ = 0.92 g/cm³, ice @ 0°C

4.1.2 Conductive Fillers

The candidate PCMs in the ambient temperature range are all thermal insulators. For use as heat storage media, a means of conducting heat into and out of the PCM matrix is needed. This may be done using high-k extended surface structures (fins) as a filler core material into which the PCM is loaded as matrix. ESLI has demonstrated [Knowles, 1987] that highly dispersing foils and fibers in a PCM matrix allow optimum use of a given volume fraction of core conductor. ESLI has been developing carbon fiber electroflocking as means of preparing high-k wick structures well suited for PCC applications.   The fin dispersion required is that for which the thermal resistance down a fin be large compared to the thermal resistance out across a PCM layer. This requirement leads to the following thickness requirement for the fins:

$$d_{fin} \ll 2 L \left(\frac{k_{PCM} \, \phi}{k_{fin} \, (1 - \phi)} \right)^{1/2} \tag{10}$$

where L is the thickness of the PCC, and ϕ is the volume fraction of the fin material in the composite, and k = thermal conductivity. Carbon fiber fins of a few millimeters length and ten micron diameter meet the requirement.

When the resistance ratio condition is satisfied, the following rule of fractions applies to the composite thermal properties:

$$k_c = k_{fin} \, \phi + k_{PCM} \, (1 - \phi) \tag{11}$$

$$c_c = c_{fin} \, \phi + c_{PCM} \, (1 - \phi) \tag{12}$$

$$H_c = H \, (1 - \phi) \tag{13}$$

$$\rho_c = \rho_{fin} \, \phi + \rho_{PCM} \, (1 - \phi) \tag{14}$$

where c is volumetric heat capacity, H is volumetric latent heat, and ρ is density. These equations describe the PCC properties for dynamic processes.

The materials having the highest room temperature thermal conductivity are shown in Table V. The best practical candidates for PCC design are the metal foils or carbon fibers. The latter are preferable for several reasons:

- high specific thermal conductivity
- better chemical compatibility with PCMs
- ease of fabrication

Table V   Specific thermal conductivity of selected high-*k* filler materials.

MATERIAL	k (W/K-cm)	ρ (g/cm^3)	k/ρ
copper	4.2	8.9	0.5
aluminum	2.4	2.7	0.9
K-1100 carbon fibers	11.	1.9	5.8
natural diamond	22.	3.5	6.3
vapor-grown carbon fibers	20.	1.9	10.5

4.1.3   Wetting Agents

PCMs change their density during melting, which can cause severe expansion stress that bursts the encapsulation. Most PCM canisters are robust (and therefore heavy) to counteract this problem with brute force. ESLI has experience with organic PCMs and dispersed metal filler structures in hermetic encapsulation where expansion stress is reduced by capillary control of the void distribution. Using this design, lightweight canisters that survive thermal cycling through the melting point are possible. The filler dispersion and the wettability of the filler by the PCM are critical in this approach.

Wetting agents are needed to make the high-*k* carbon fibers wettable. Pure water does not wet high-*k* carbon fibers, but soapy water does. The following are recommended surfactants for the carbon-water system:

- Actrasol ŞBO (Climax Performance Materials)
- Amphoteric 400 (Exxon Chemical)
- Alkali Surfactant NM (Exxon Chemical)
- Dowfax 2A1 (Dow Chemical)
- Zonyl FSN (DuPont)

The minimum amount of surfactant is desired to minimally disrupt the crystal structure and possibly decrease the effective latent heat.

These surfactants were first tested by determining the concentration in water required to enable a tow to be fully wetted to a height of 3 cm. The surfactants were also tested by measuring the diameter of a 50 microliter drop of 0.10% aqueous solution deposited on a clean piece of graphite foil (Grafoil GTA). Table VI summarizes the results.

Table VI   Test results of surfactants recommended for wetting carbon.

SURFACTANT	amount required in water to wet carbon fibers (vol %)	diameter of 50 μL of 0.1% solution placed on Grafoil (cm)
(no surfactant)	--	0.64 $\pm$ .02
Amphoteric 400	> 1.2	0.64 $\pm$ .02
Alkali NM	0.15	0.70 $\pm$ .01
Dowfax 2A1	0.08	0.79 $\pm$ .02
Actrasol SBO	0.10	0.83 $\pm$ .02
Zonyl FSN	0.02	0.96 $\pm$ .03

Based on these results the following surfactant was selected: 1 part Zonyl FSN plus 4000 parts distilled water. Zonyl FSN consists of 30% water, 30% isopropanol, $\approx$40% perfluoroalkyl ethoxylate, and <0.1% 1,4-dioxane. It presents the lowest toxicity hazard of the five surfactants considered.

4.2   PCC Component Fabrication

4.2.1   Preliminary Capillary Control Tests

An example of freezing stress problems is the behavior of water pipes in cold climates. Water expands roughly 10% when it freezes. An exposed exterior faucet that freezes in cold weather develops a plug of interior ice that expands and presses on the water in the pipe. The mounting pressure with increasing ice growth can rupture thick pipes. Water confined to its original volume will generate on the order of 180 MPa (25 ksi) of expansion pressure while freezing.

To avoid such failures, adequate void volume must be accessible to the expanding ice. In PCC capsule design, adequate void space in the encapsulation is provided to allow for expansion (plus some margin of safety). That is simple. The challenge is to assure that little or none of the available void space can get trapped as bubbles inside the ice while it forms. For example, an open beaker placed on a cold plate can freeze from below without a problem. If the beaker is replaced with a closed metallic can, problems arise because the top of the fluid develops a crust that encapsulates voids and makes them inaccessible. These problems are aggravated in the absence of gravity.

Capillary fluid retention - A conductive filler is required to ensure adequate heat transfer, and, if properly dispersed, it can also control PCM fluid and void distribution. For this application

carbon fibers are preferred because they are light, strong and have higher specific thermal conductivity than any other material in this temperature range. Electroflocking permits the fabrication of high-k wick structures of suitable dispersion.

Capillary tube experiments - We initially studied the freezing behavior of water in capillary tubes, with and without carbon fibers. Each capillary tube had the following specifications: ID = 0.14 cm; wall thickness = 0.023 cm; length = 5.2 cm; total cavity volume = 0.08 cm^3.

Filling and sealing was performed as follows: one end of the open tube was sealed with 5-minute epoxy; the tube was then filled with distilled water by vacuum backfill; the vertical tube was then frozen slowly on a controlled cold plate; the open end was then sealed by placing a small ball bearing on the tip and bonding with 5-minute epoxy. The tube was completely filled with ice, but after melting it was observed to have approximately 9% void volume. This void volume consisted of one or more large bubbles that could be made to move in response to tilting or tapping.

The carbon fiber-filled tube contained 8,000 P-120 carbon fibers and distilled water to which a soap ("Now" detergent of unknown composition) was added at 0.15% volume concentration. This concentration ratio was the minimum required to get complete wetting of the carbon fiber tows along their whole length when held up vertical. Filling and sealing was performed as above. In this case the voids consisted of many small bubbles near the tube wall, and they were less mobile.

The tubes behaved very differently upon freezing. Each tube initially at room temperature was placed horizontally on an aluminum cold plate held at -23±3 °C. A clear polycarbonate splatter shield was placed over the capillary tube, without contacting it. The two capillary tubes without carbon fiber packings fractured dramatically during the first freeze cycle. The reason this happens is that ice tends to form around the voids first (they have less heat capacity and get colder faster than the surrounding fluid). These voids are then inaccessible as the remainder of the water freezes. Water that freezes later and expands finds no voids for relief and builds pressure that eventually bursts the tubes.

The tube with the carbon fiber packing survived 15 deep thermal cycles without failure. The cycles consisted of placing the tube in warm water to heat and then back onto the cold plate to cool. The voids noticeable at the tube walls gradually shrank away as freezing progressed. This tube also survived deep cycling in vertical orientation (inserted into a small blind hole in the plate).

Capsule experiments - Two capsules were fabricated with the following characteristics:

height:	3.81 cm
diameter:	1.27 cm
end plates:	aluminum, 0.318 cm thick
cross pin:	both capsules had a 4-40 screw penetrating crosswise midway between the end plates
capsule #1:	no fibers; 87.5% filled with distilled water
capsule #2:	upper 90% of interior packed with carbon felt bonded to the upper end plate; 87.5% filled with distilled water

Capsule #1 performed well when frozen from below. In this case the ice forms and lifts liquid water, gradually filling the void at the top. However, when frozen from the top surface, the capsule ruptured during the first freeze cycle. The reason for this is that the void at the top became encapsulated with ice before it totally shrank, leaving some void inaccessible to water that later expanded as it froze. The cross pin was used to prevent slippage of the ice plug.

Capsule #2 did not rupture under either freezing process. When the capsule was frozen from above, the capillary forces held the liquid above the voids, and the freezing water could expand without resistance. The void space at the lower end of the cell was observed to shrink from above as liquid water was extruded into the space. The freezing of this thin layer of water from the top caused no failure.

4.2.2 Subscale Sleeve Fabrication

Subscale sleeves for testing - A 1/4-scale sleeve design was selected for further testing. A series of subscale sleeves was fabricated and are shown in Figure 5. The inside tubes are either acrylic or aluminum, 2.54 cm OD. The outside tubes are all acrylic, having 3.18 cm ID, 3.81 cm OD. The interior gap is 0.318 cm (0.125 inch). The amount of PCM (water or tetradecane) required for fill was determined gravimetrically by weighing the evacuated sleeve, vacuum backfilling the cavity entirely with PCM and reweighing, and then using a syringe to extract the excess PCM. The fill fraction selected for water is 87.5%; the fill fraction for the tetradecane is 98%.

4.3   Phase-Change Thermal Cycling

Freeze-melt cycle testing - A thermal cycle bench was designed (Figure 6) to perform cycling in which cooling occurs through the inner sleeve only. This choice is consistent with the assumption that, in the battery application, the conductive sleeve liner will be connected to the heat sink. In this configuration heat is removed from the sleeve at the metal post whose temperature is set by a digital temperature controller. The heat sink is a liquid nitrogen reservoir and heat for temperature control is provided by the electrical resistance wire wound tightly onto the post. The cold temperature used for freezing is -20°C ± 2°C. For melting, the sleeve was removed from the post and warm air (approx. 50°C) was blown down the central hole. Of primary interest is in the freezing phase, when the stress problems arise with water. The melting phase does not cause problems.

The summary results of cycle testing are shown in Table VII:

Sleeve No. 1 - Acrylic tubing with 3 mm (0.125") thickness was used to form a sleeve with a 3 mm (0.125") thick internal gap for water. The overall sleeve dimension was 18 mm ID and 36 mm OD. Water to 87.5% fill fraction was added and the sleeve sealed with a cemented plastic screw. This entirely acrylic sleeve has poor heat transfer but does not fail during thermal cycling. When placed vertically in a freezer, for example, ice initially forms on both walls expanding inward toward the gap. The water gradually extrudes upward in the gap. Eventually all the water freezes without developing excessive stress, because the voids needed for expansion remain accessible.
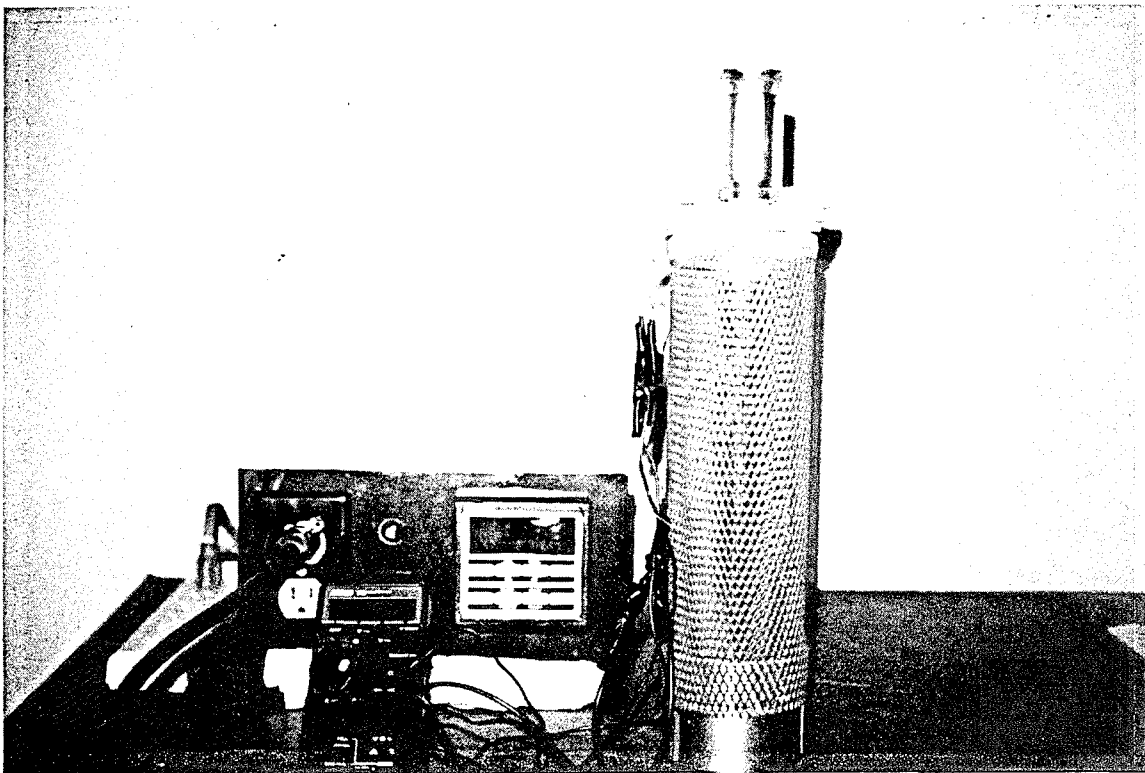

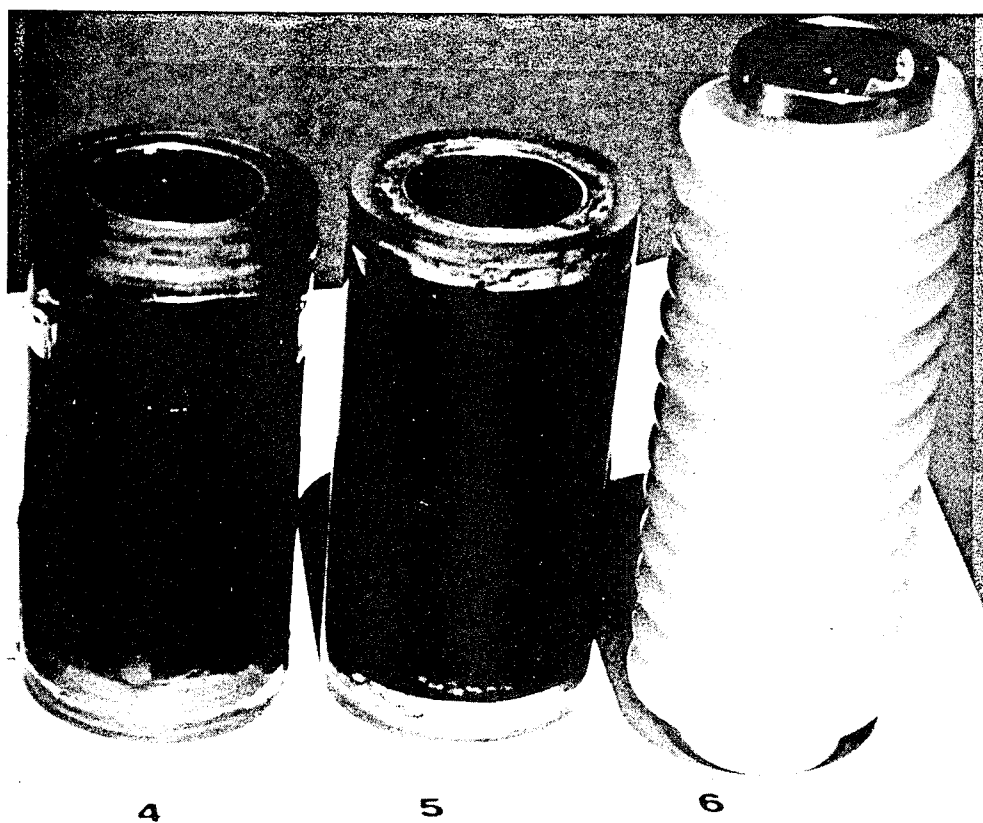**Figure 6**   Photo of thermal cycling bench for subscale sleeve testing.
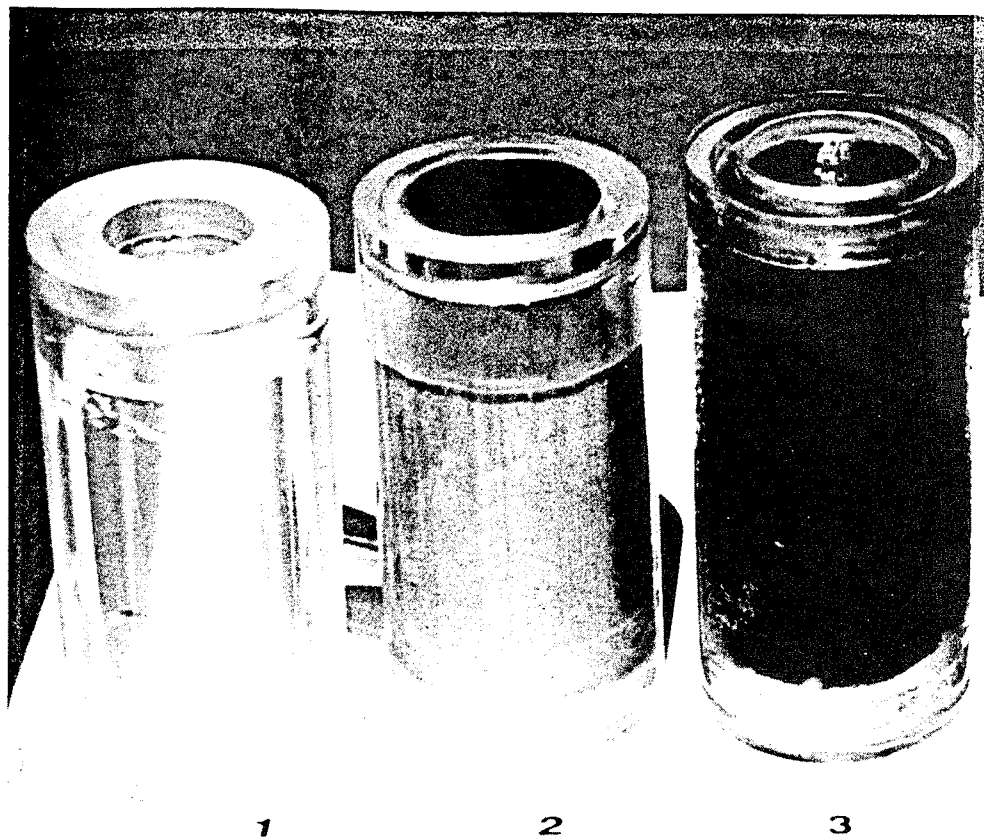
Figure 5   Subscale sleeves Nos 1. - 6.

Sleeve No. 2 - An aluminum tube with 1.0 mm (0.04") wall thickness was used for the inner cylinder. The rest of the sleeve was acrylic. This sleeve survived vertical cycling, but failed during the first horizontal cycle. A thick ice dam formed quickly around the void at the top of the horizontal cylinder, because of the large area of unwetted aluminum that served as a cold fin to freeze the void boundary. The trapped voids were inaccessible to the remaining water and a rupture at the end seal occurred.

Table VII Summary of cycle test results. The Precision Flocked Aluminum Sleeve design has best survived thermal cycling with water.

Sleeve	Materials			Cycles		Fail	Comments
	inner cylinder	outer cylinder	PCM	vert-ical	hori-zont.	?	
1	acrylic	acrylic	water	5	5	No	slow to freeze, low conductivity
2	aluminum	acrylic	water	5	1	Yes	ice slides in vertical tube
3	flocked aluminum	acrylic	water - 87.5% full - 85.0% full - 80.0% full	 1 1 1	 0 0 0	 Yes Yes Yes	uneven flock traps voids; always fails
4	precision flocked aluminum	acrylic	water	5	0	Yes	bald spots in flock at ends; gradual weakening of seals
4 mod.	precision flocked aluminum	acrylic	water	6	5	No	filled bald spots in flock on Sleeve No. 4 with epoxy
5	precision flocked aluminum	acrylic	tetradecane	5	5	No	tested in freezer only
6	aluminum tube; helical wrap of polyethylene tubing		water	20		No	30 cm x 6 mm closed tube; tested in freezer

24

Sleeve No. 3 - A sleeve was fabricated like No. 2, except that the inner wall was electroflocked with AMOCO P-120 carbon fibers coarsely cut to ≤3 mm length. During the vertical freeze cycle the sleeve ruptured at the top end. This failure was apparently caused by numerous small void bubbles trapped in ice against the outer wall. Occasional groups of long fibers reached completely across the interior gap and formed small pockets of voids surrounded by ice. The trapped voids are inaccessible to the remaining water and stress arises at some later stage of freezing when water needs to expand but does not have adequate room.

The top of this sleeve was re-cemented, and the water fill fraction was reduced in an effort to provide more void volume. The new version also failed at the first freeze attempt for the same reason. Again we reduced the fill fraction, and again the same failure occurred. At each stage, the trapped voids increased in size and at 80% fill the testing was terminated.

Sleeve No. 4 - Another flocked sleeve was fabricated like sleeve No. 3 except that *precision cut* AMOCO P-120 fibers having length 2.4 mm were used. An example of flock prepared from such precision cut fibers is shown in Figure 7. These fibers were flocked onto the aluminum inner sleeve such that a clear gap of approximately 0.5 mm resulted between the fiber tips and the outer wall. This sleeve survived 5 cycles on the cycle bench, but failed on the 6th cycle by a small leak at the tip. We attributed this to an unflocked "bald" region at the ends in which the last of the water freezes. It seems that this small annulus of water would develop some stress. It may also be that water crept into fissures between the sealing collar and the cylinders where it froze and increased the fissure size until failure occurred.

Sleeve No. 4, modified - Sleeve No. 4 was modified by first removing the water, adding a layer of epoxy inside to fill the bald, non-fiber areas at the tube ends, and then refilling to 87.5% water fill fraction. This sleeve was then repeatedly cycled on the cycle bench and in the freezer in various orientations. It did not fail. It appears quite robust and the total weight of 72.37 g has not changed during testing.

The reason this sleeve survives cycling so well is that the void location is completely controlled by the flocked fiber "wick". Capillary action in the flock wick keeps the cold surface wetted and prevents void bubbles from being trapped leading to problems at later stages of freezing.

Sleeve No. 5: organic PCM - Another flocked sleeve was fabricated like the modified No. 4, but it was filled to 98% with n-tetradecane, the organic PCM recommended for study. This structure has survived thermal cycling without sign of failure. Organic PCMs are generally easier to work with because they develop less mechanical stress: their solid phase is softer than ice. Stress can develop when the organic PCM melts and expands. It appears that the expanding liquid merely pushes between fibers in the flock felt and extrudes to the gap region between the fibers and the outer wall.
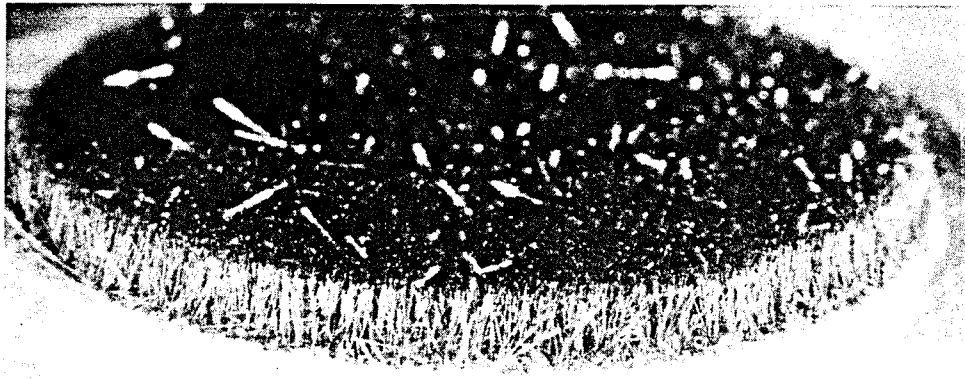
Figure 7   Photo illustration of flocked precision cut carbon fibers, 1.25 mm long.

Sleeve No. 6: polyethylene tubing - A simple design that may be adequate for low rate discharge batteries is to wrap polyethylene tubes around a metallic sleeve. The behavior was tested for a length of such tubing filled with water and having the following dimensions length = 30 cm (12"), outside diameter = 6.3 mm (0.25"), wall thickness = 0.10 mm (0.040"). The tube was completely filled with water, sealed at both ends, and cycled by placing it in a freezer at -10°C for one to ten hours and then removing to room temperature. We observed that the expansion of ice is well accommodated by the elasticity of the tubing and, after at least twenty cycles, no failures were observed. The frozen tube remains moderately pliable: a quick twist by hand of the frozen tube shatters the ice "noodle" inside the tube. It seems the tubular design is a simple, low cost design that indeed survives thermal cycling. In spite of its poor thermal conductivity, is recommended for further comparative testing with other sleeve designs.

Conclusions - We have demonstrated that PCC sleeve structures loaded with either tetradecane or water as the PCM do survive freeze/melt cycling. Finding a way to utilize water without the threat of bursting the encapsulation is important, because water is in many respects the preferred PCM.

4.4   Prototype Design Options

Sleeve geometry - The cylindrical sleeve geometry is a likely PCC configuration for use with individual pressure vessel (IPV) Ni-H$_2$ cells. The PCC sleeve would replace the existing sleeve

completely. It therefore must meet structural as well as thermal requirements. Sizing based on total heat dissipated gives a sleeve thickness of approximately 6 mm (0.24"). Table VIII shows the sleeve dimension under the assumption that 50% of the sleeve is wall thickness. This assumption is very conservative and, in fact, the actual sleeve may well be thinner.

The thermal conductivity requirement may be estimated by considering the Eagle-Picher RNH-78 cell (Table II) that dissipates 10 W. If the power is assumed uniformly distributed over the entire vessel, there will be a temperature difference of approximately 7 K through a 6 mm sleeve having k = 0.2 W/m-K. By using a 1% volume packing fraction of radial carbon fiber fins, this temperature difference should reduce gradient to less than 1 K. The cell-sleeve thermal contact resistance becomes the dominant effect.

Sleeve design options are:
- metallic sleeve liner with carbon fiber wick
     Issue: corrosion of aluminum and carbon fibers
     Issue: weight of copper liner

Table VIII   Sample sleeve dimensions and heat capacity enhancement. Assume PCM heat capacity only 50% as large as water to account for encapsulation penalties.

Sleeve

length =	15.24	cm
inside diameter =	8.89	cm
outside diameter =	10.16	cm
sleeve volume =	289.6	cm3
sleeve volume / cylinder volume =	30.6%	

Ni-H2 Cell

heat capacity =	1.74	kJ/K
temperature change =	10	K
cell heat change =	17.4	kJ

PCM

latent heat =	167	J/cm3
specific heat =	2.09	J/K-cm3
sleeve heat capacity =	18.785	J/K-cm3
sleeve heat change =	54.40	kJ

Heat Capacity Enhancement

total heat capacity/cell heat =	4.13	(multiple)

Issue: strength of fiber composite liner
- polymer matrix composite sleeve liner with carbon fiber wick
- helical polyethylene tubing
  Issue: thermal conductivity and time scale
- helical metal fin on metal sleeve liner
  Issue: corrosion of aluminum
  Issue: void distribution control; expansion stress
- longitudinal aluminum fin on aluminum sleeve liner

The outer encapsulation, which may be insulating, can be a simple polymeric or polymer matrix composite material.

Carbon-carbon sleeves - For use in Na-S batteries, the sleeve must tolerate high temperatures ~ 300°C where aluminum is weak. Carbon-carbon is a candidate material and the encapsulation of PCMs in conductive carbon tubes is an option. The tubes may be integrated in the carbon-carbon matrix. A similar concept has been implemented in a high temperature carbon brake application [Knowles, 1993].

Interior PCC - For cell-interior locations, especially in the CPV batteries, the leading candidate PCC configurations are:
- flat plates separating the polybag cells (in CPVs)
- annular jackets on the inside wall of IPVs
- rods on the axis inside multicell CPVs

PCC baseplates - The simple baseplate option is thermally less desirable, because the PCM is placed a greater distance from the cell interior where the heat is dissipated. There may be designs, however, where the baseplate is the preferred location for the PCC material. It does have the advantage of being comparatively simple to retrofit and perhaps easier to qualify.

PCC plates would presumably be easier to fabricate than PCC sleeves. They would likely consist of a high-k honeycomb core with carbon fiber wick structures on the honeycomb cell walls, reaching essentially to the cell axis. This design has not been implemented, but is recommended based on the above successful testing of carbon fiber wick structures in subscale sleeves.

4.5   Full-Scale Sleeve Fabrication

A full-scale sleeve, 18 cm x 10 cm was fabricated for illustration purposes. It consists of an aluminum inner liner onto which AMOCO P-120 radial carbon fiber wick has been electroflocked to approximately 1% packing fraction. The outer cylindrical shell and the close outs at the ends of the cylinder were made of lucite. The interior was 85% filled with our preferred solution distilled water and surfactant. The resulting structure has been used for illustration purposes and not subjected to thermal cycling. The full-scale PCC sleeve is shown in Figure 8.
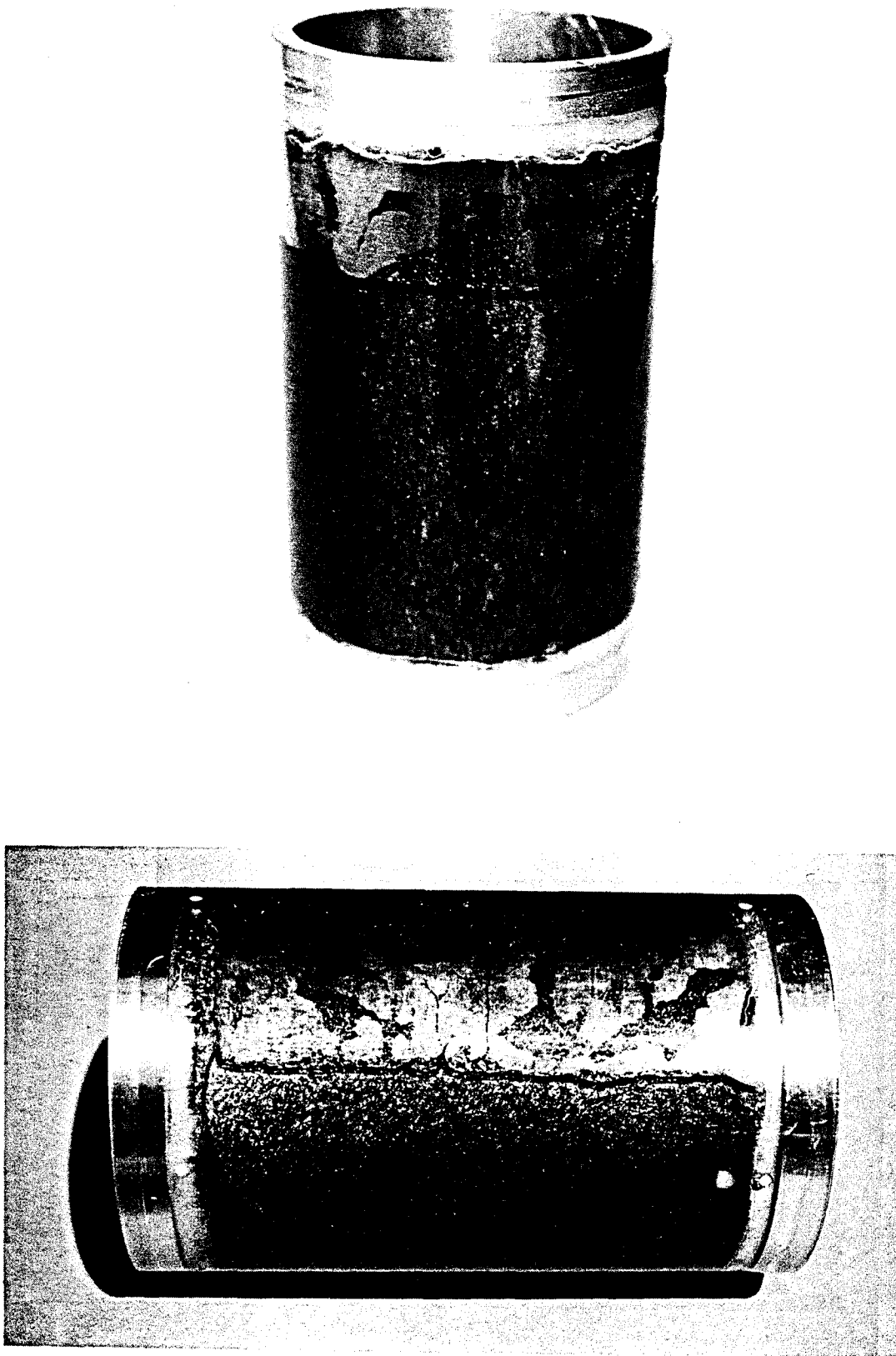
Figure 8   ESLI PCC sleeve Model No. 001. Full scale for EPI 80 Ahr Ni-H2 cell. Vertical and horizontal views.

5   THERMAL ANALYSIS

To investigate in greater detail the performance and mass trade-offs of thermal energy storage, radiators and heaters, a simple two-node system model is developed. The model is solved analytically for the special case of simple periodic heat dissipation. The model is then solved numerically for arbitrary battery heat dissipation and heater power. GEO applications are investigated in detail and it is shown that using PCC allows an improvement in temperature control and a savings in heater power. A significant net reduction in system mass and size is enabled by PCC in this application. Surge mode LEO cases are briefly considered. Finally a detailed multinode thermal analysis of the axisymmetric sleeve is developed to investigate the time-dependent temperature distribution in the PCC sleeve.

5.1   Two-Node System Model

5.1.1   Model Definition

A simple two-node system model gives interesting qualitative understanding of the role of the radiator, the active heaters and TES on space battery thermal control. The two-node thermal model is illustrated in Figure 9. The capacity of the battery cells and the PCC are combined into one node, because they are rather strongly coupled. The radiator is sized for the average power dissipation using the Stefan-Boltzmann Law and the transients are determined using a linearized form of that law,
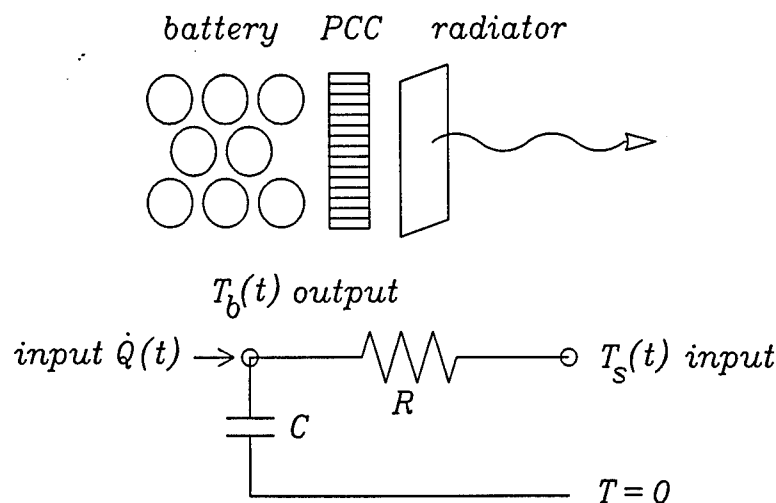

Figure 9   Thermal system schematic and two-node circuit model.

30

in which it acts like a simple thermal resistance coupling the battery to space. The objective is to determine the battery temperature

$$T_B(t) = T_B + \Delta T_B(t) \qquad (15)$$

for boundary conditions in which the battery and the heaters dissipate a given heat power and the space temperature is specified:

$$\dot{Q}(t) = \dot{Q} + \Delta\dot{Q}(t) \qquad (16)$$

$$T_S(t) = T_S + \Delta T_S(t) \qquad (17)$$

The simple thermal circuit in Figure 9 is solved in the same manner as the more commonly studied electrical circuit version. The heat current is conserved at the battery node and the total temperature drop around any loop in the circuit equals zero. The resulting equations for the general time-dependent terms may be expressed as follows:

$$\Delta\dot{Q}_C + \int_0^t \frac{\Delta\dot{Q}_C(t')}{R\,C}\,dt' = \Delta\dot{Q} + \frac{\Delta T_S}{R} \qquad (18)$$

$$\Delta T_B(t) = \int_0^t \frac{\Delta\dot{Q}_C(t')}{C}\,dt' \qquad (19)$$

where $\Delta\dot{Q}_C$ is the heat current into the capacity.

Sleeve capacity - The effective capacity of a PCM is the sum of the intrinsic, so-called "sensible" heat capacity and the latent heat capacity. The latent heat of fusion transfers in the melting point range, which is generally small compared to the temperature changes typically experienced in a battery. For modeling purposes, it is a useful approximation to treat the latent heat as spread out over the whole temperature range ΔT, in which case its effective heat capacity contribution is $H/\Delta T$. The total effective heat capacity is then

$$c_{eff} = c + \frac{H}{\Delta T} \qquad (20)$$

For example, water has $H = 334$ J/cm^3, and the effective heat capacity of the PCM from just below the freezing point to 10°C above is

$$c_{eff} = 4.17 + 33.4 \approx 37.6 \quad J/cm^3 \qquad (21)$$

For small ΔT, PCMs have high effective high capacities; compare the above value with the sensible heat capacity of water, $c = 4.17$ J/cm^3.

The increase in heat capacity provided by a PCC sleeve can be a multiple of the cell heat capacity, even for rather thin sleeves. For example, assume that 50% of the total sleeve volume is filled with PCM and the remainder consists of wall material. This is likely to be an underestimate of the PCM fraction. Figure 10 shows the heat capacity enhancement for various sleeve thicknesses and battery temperature changes, assuming water as the PCM. A sleeve length of 6 in was assumed. Note that modest sleeve thicknesses allow a multiple enhancement of the battery heat capacity.

Radiator - To assess the performance and mass tradeoffs of radiators and PCC in batteries, the effect of sizing the radiator is considered. The power, $\dot{Q}_{rad}$, radiated from a flat surface viewing space is given by

$$\dot{Q}_{rad} = \epsilon \sigma \int dA \ (T^4 - T_s^4) = \sigma A^* \ (T^4 - T_s^4) \tag{22}$$

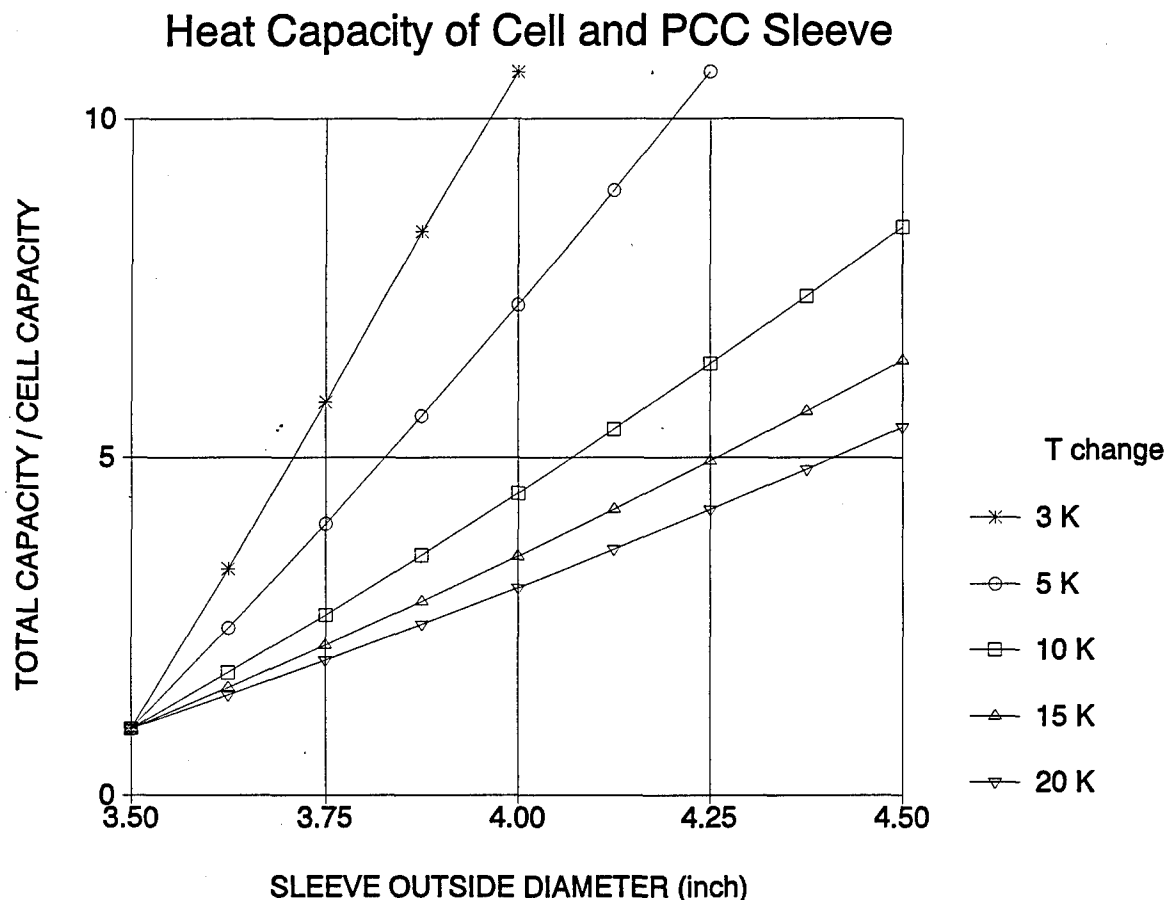## Heat Capacity of Cell and PCC Sleeve

Figure 10 Heat capacity enhancement of PCC sleeves of various thicknesses for several battery temperature changes. Water at 50% fill fraction is assumed for the PCM.

32

where the Stefan-Boltzmann constant $\sigma = 5.67 \times 10^{-8}$ W/K^4-m^2. The effective area A^* is defined by the above equation. We also define the effective radiator conductance, having units of W/K-m^2, as follows:

$$h = \frac{1}{A^*} \frac{\partial \dot{Q}_{rad}}{\partial T} = 4 \sigma T^3 \tag{23}$$

The latter quantity is useful in calculating the change in radiated power, per effective area, for a small change in radiator temperature.

Figure 11 shows the radiated power and conductance for parameters $A^* = 1$ m^2 and $T_S = 200$ K. Observe, for example, that at 0°C the radiated power is 224 W, and this power drops by roughly 50% if temperature is lowered by 30°C.

Simple periodic heat dissipation - For the special case of a simple harmonic heat dissipation (superposed on a steady-state heat dissipation) the driving term is given by

$$\dot{Q}(t) = \dot{Q} + \Delta\dot{Q} \, e^{i\omega t} \tag{24}$$

Space Radiator Performance

Space T = 200 K; effective A = 1 m2

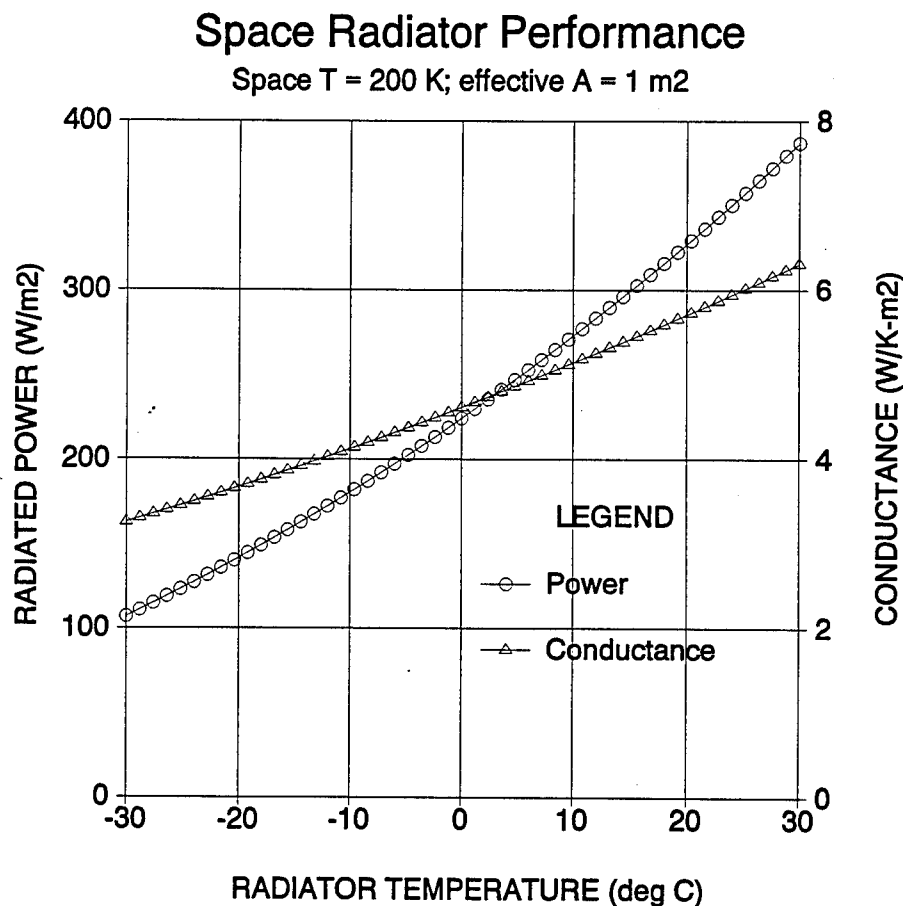**Figure 11**   Radiated power and conductance of space radiator vs temperature near 0°C. $T_S = 200$ K.

The solution of Eqns. (18) and (19) is

$$T_B = T_S + \dot{Q} R \tag{25}$$

$$\Delta T_B = \Re \left\{ \frac{\Delta \dot{Q} R + \Delta T_S}{1 + i \omega R C} \right\} \tag{26}$$

where the term in braces is complex, containing both magnitude and phase information, and $\Re$ signifies that the real part is required. If the space heat sink temperature is constant, $\Delta T_S = 0$, then

$$|\Delta T_B| = \frac{\Delta \dot{Q} R}{[1 + (\omega R C)^2]^{1/2}} \tag{27}$$

The heat transferred to space by the radiator is given by the usual T^4 expression, and the associated resistance R is given by

$$R = \frac{1}{\partial P_{rad} / \partial T} = \frac{1}{4 \sigma \epsilon A_o T^3} \tag{28}$$

Note that the resistance is inversely proportional to the radiator area, and the mass generally scales with the area. Mass trades are made by comparing the radiator mass and the PCC mass required to maintain a given maximum ΔT_B, while minimizing system weight.

Consider an aluminum radiator 2.5 mm thick with a specific mass of 6.75 kg/m². Couple this radiator with an Eagle Picher Battery #10017 RNH 78-1 whose thermal specifications are shown in Table IX. The model predicts the radiator mass required for given ΔT_B when no PCC is used, and it predicts the mass of PCC required when only the basic radiator is used. Figure 12 shows a graphical comparison of the mass required for the parameter case shown in Table X. On a weight basis, PCC is more effective than radiators at reducing temperature variations in the battery in this model.

Table IX   Nickel-hydrogen battery thermal specifications.
               Eagle-Picher Industries #10017, RNH 78-1 Space Battery.

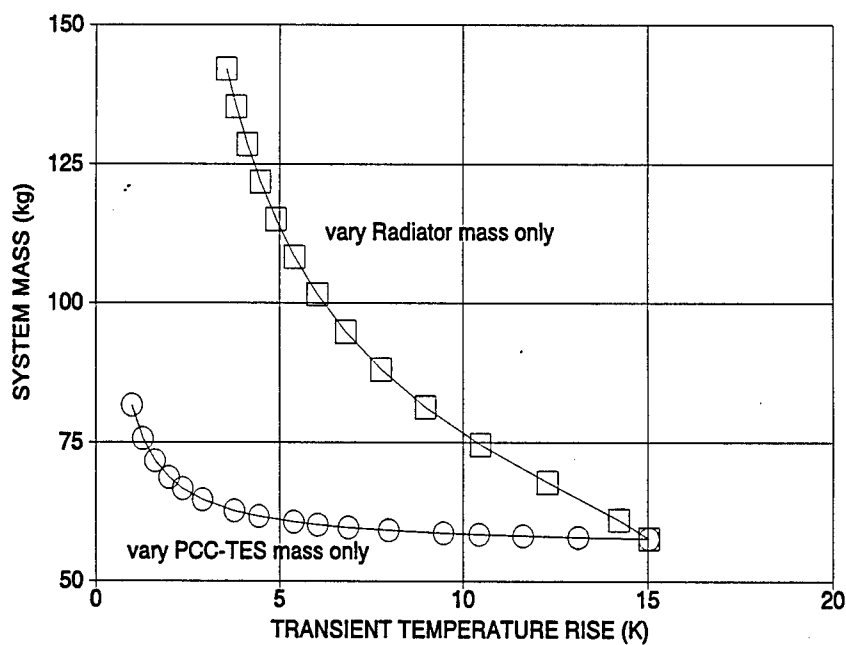|		
cell dissipation, discharge	(W)	10
number of cells		27
discharge time	(s)	4200
energy dissipated	(MJ)	1.134
cell mass	(kg)	1.886
battery mass	(kg)	68.8
cell heat capacity	(J/K)	1741
cell specific heat	(J/kg-K)	923.1
battery+radiator temperature rise	(K)	17.86
cell temperature rise	(K)	24.12

Figure 12   Using PCM to lower peak temperatures results in a comparatively small mass penalty for 27-cell nickel-hydrogen GEO battery.

Table X   Parameters used in two-node model calculation.

The orbit:		
discharge period =	4.8	hr
omega =	0.000364	1/s
The radiator:		
$\epsilon\sigma$ =	5.10e-08	$W/K^4\text{-}m^2$
radiator area A =	**1.00**	m^2
avg batt T =	300	K
average space T =	200	K
average radiated power Q =	332	W
radiator R =	0.181	K/W
radiator areal mass =	6.75	kg/m^2
The battery:		
battery M =	**50.9**	kg
battery specific heat c =	0.923	kJ/kg-K
battery heat capacity C =	47.0	kJ/K
average battery dissipation =	--	W
variable battery dissipation =	**270**	W
The TES:		
TES M =	2	kg
TES specific heat c =	35	kJ/kg-K
TES heat capacity C =	70	kJ/K
The temperature variation:		
ωRC =	7.72	-
delT =	**6.29**	K
total M =	**59.672**	kg

5.1.2 Numerical Solution

To solve the two-node model for more realistic, non-harmonic heat generation profiles, the governing equations are expressed in dimensionless form. Define

$$\Delta \dot{Q} = P_0 \, q(\tau) \tag{29}$$

$$\tau = \frac{t}{R \, C} \tag{30}$$

$$x = \frac{\Delta \dot{Q}_C}{P_0} \tag{31}$$

$$y = \frac{\Delta T_s}{R \, P_0} \tag{32}$$

Then Eqns (18) and (19) give

$$a \equiv \frac{R \, C}{P_0} \frac{\partial}{\partial t} \left\{ \Delta \dot{Q} + \frac{\Delta T_s}{R \, C} \right\} = \frac{\partial}{\partial \tau} \left\{ x + y \right\} \tag{33}$$

After differentiating once

$$\dot{x} + x = a \tag{34}$$

The time-varying terms average to zero by definition, so that

$$\int_{period} \Delta \dot{Q} \, d\tau = 0 \tag{35}$$

Rewriting Eqns. (33) and (34) as difference equations gives

$$a_n = \frac{q_n - q_{n-1} + y_n - y_{n-1}}{\Delta \tau} \tag{36}$$

$$x_n = \frac{x_{n-1} + a_n \, \Delta \tau}{1 + \Delta \tau} \tag{37}$$

Assuming that space temperature is constant for simplicity, Eqns. (36) and (37) reduce to

$$x_n = \frac{x_{n-1} + q_n - q_{n-1}}{1 + \Delta \tau} \tag{38}$$

and we have the condition

$$y_n = \sum_0^n x_{n'} \Delta \tau = 0 \tag{39}$$

Solving these difference equations is straightforward. Solutions were generated using a spreadsheet program PlanPerfect v5.1 from the WordPerfect Corporation. This spreadsheet was used for convenience, but it is not recommended for more complicated models having several nodes.

Dependence on R, C - The difference equations were solved for the Eagle-Picher RNH-78 Ni-H$_2$ battery + radiator system (parameters provided by J. Dermott, EPI). Figure 13 shows the temperature variation, ΔT_B, around the average T_B, for three cases:

1. baseline case: 1 m^2 radiator, intrinsic battery heat capacity (47 kJ/K)
2. high-capacity case: baseline radiator and 3x higher heat capacity
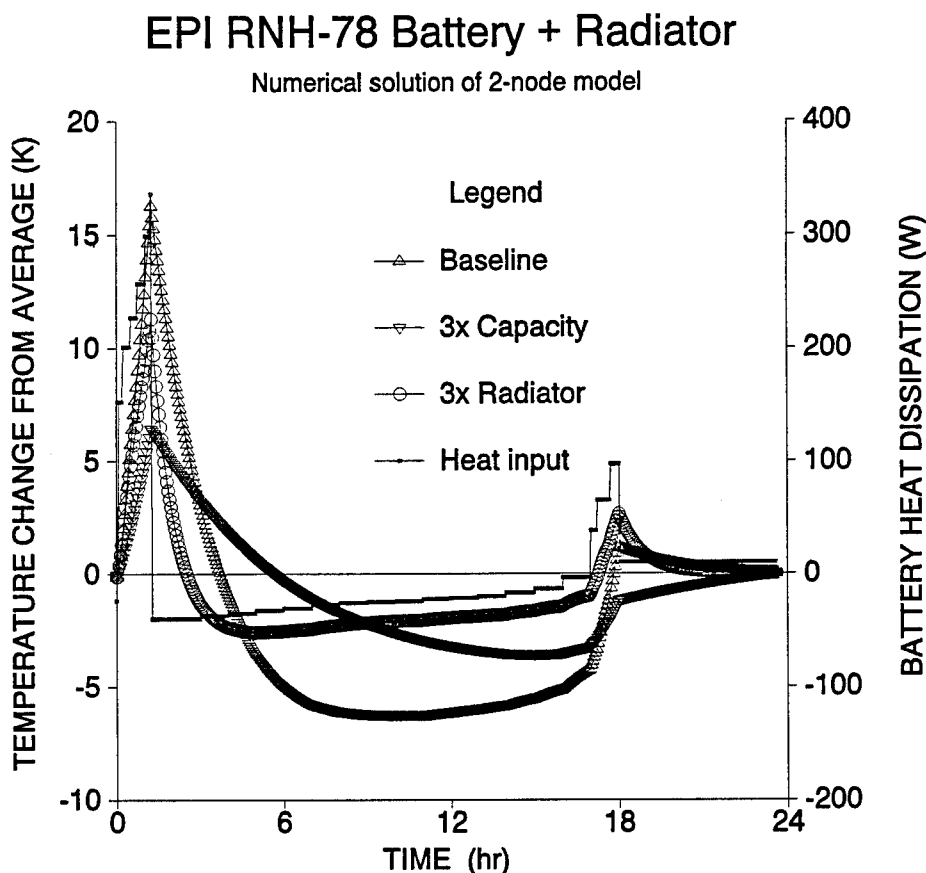3. low resistance case: 3x larger radiator and baseline heat capacity

Figure 13 Temperature response of battery with 3x increased radiator and with 3x increased heat capacity.

38

Increasing the size of the radiator as well as increasing the heat capacity of the battery improves temperature control. The weight of the PCC heat capacity enhancement is roughly 15% that of the weight of the large radiator . The model assumes a perfectly efficient radiator as well as perfect thermal coupling of the PCC heat capacity to the cell.

Figure 14 compares the performance of the baseline case with a system having half as much radiator area and a quantity of PCC that corresponds to $3x$ the battery heat capacity, making a total of $4x$ the baseline heat capacity. Such heat capacity is easily accommodated in a 3/8" sleeve thickness. The half-sized battery, with area 0.5 m², is fully capable of heatsinking the average power (< 30 W) and the increased capacity has spread the heat dissipation over a longer time scale. The weight is roughly unchanged, but the temperature control is greatly improved: the temperature variation is 7.8°C compared to 22.1°C for the baseline case.

The benefits of PCC in this configuration are seen to be:
- improved temperature control (for improved battery cycle life)
- 50% smaller radiator, consuming less satellite resource
- less battery heater power required

EPI RNH-78 Battery + Radiator

Numerical solution of 2-node model

Legend

—△— Baseline

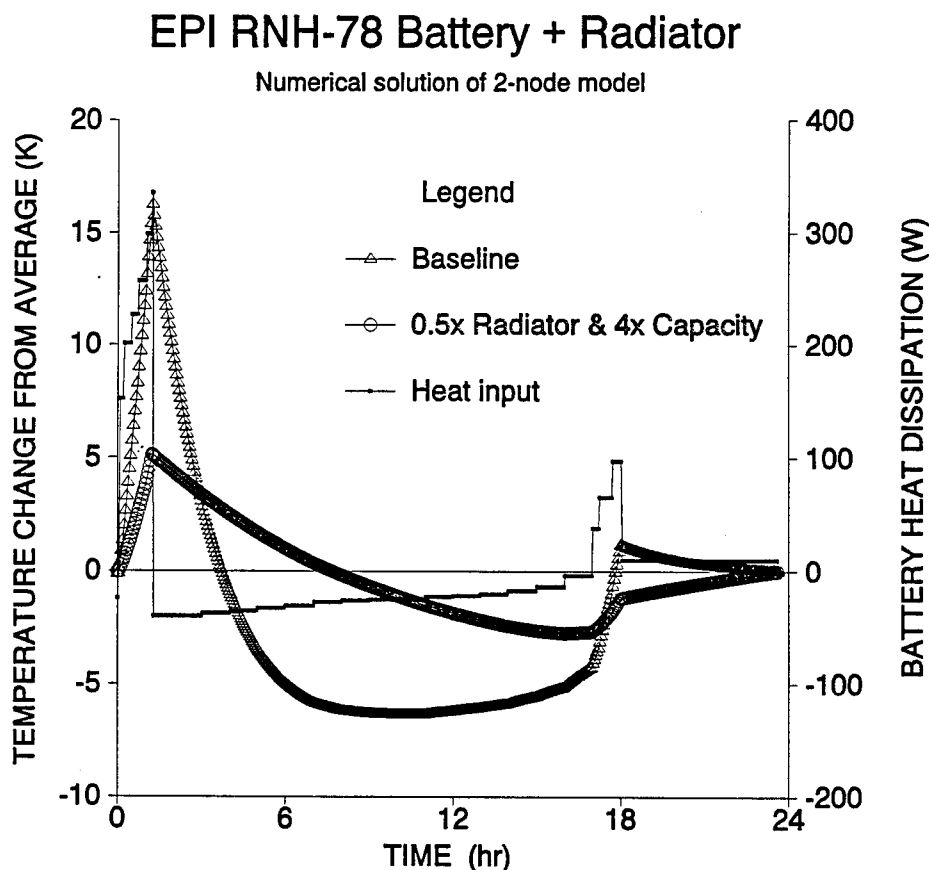—⊖— 0.5x Radiator & 4x Capacity

—— Heat input

Figure 14   Temperature response of battery with 0.5x smaller radiator and 4x increased heat capacity. The weight is roughly unchanged from the baseline case, but the temperature variation is reduced from 22.1°C to 7.8°C.

39

5.2 Numerical GEO Eclipse Simulations

5.2.1 Intelsat Battery

Intelsat battery thermal behavior was investigated. Data (LORAL, 1993) and ESLI calculations are compared in Figures 14 and 15. Fair agreement exists between the temperature profiles in these two charts. Note that the calculations in Figure 16 do not show absolute temperature, rather the deviation of temperature from the average value.

Inclusion of heater power - The previous calculations did not include heater power, primarily because no heater power data had been received. Externally applied power enters through the q-term in Eqn. (36) and its inclusion does not complicate the calculation significantly.

Parameters used - The parameters assumed for modeling purposes are:

1 IPV Ni-H_2 configuration: c_p = 1.0 J/g-K
2 orbital average battery heat dissipation = 2 W/cell (200 W)
3 orbital average heater power = 2 W/cell (200 W)
4 radiator temperature is calculated from the average power according to

$$T = 273 \ K - R \ P \tag{40}$$

with R = 0.067 K/W. Note that this R value corresponds to a 20 K gradient between battery and
   radiator for steady state heat dissipation of 200 W.
5 radiator area is determined using above temperature and assuming ϵ = 0.8. The radiator thermal
   resistance (used in model calculation) is determined by linearizing the Stefan-Boltzmann
   expression as follows:

$$R = (\frac{\partial P}{\partial T})^{-1} \tag{41}$$

Thermal control with increased DOD - Thermal control with PCCs enable the use of deeper DOD. Consider a case where the capacity of each cell is reduced by a factor two, and the DOD is doubled for the same power. The two-node model was used to calculate temperatures for the following four cases:

1   no heaters, minimum size radiator
2   no heaters, minimum size radiator, PCC to increase capacity 1000%
3   200 W (avg) heater power, normal size radiator
4   400 W (avg) heater power, twice normal size radiator

The results in Figure 20 show that the PCC option (case 2) gives very good temperature control. The weight savings involved are stunning:

- the cell mass is reduced by 50%
- the entire PV heating is eliminated
- the radiator is downsized by 60%
- the required PCM weighs only 18% of the original battery mass.
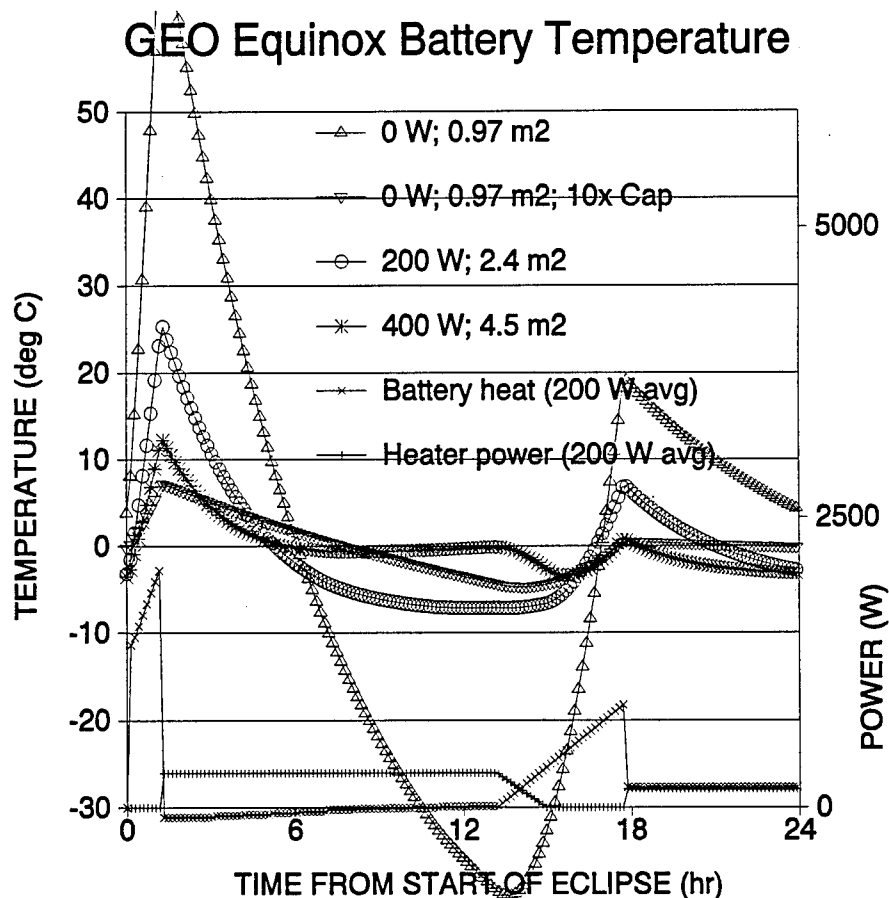

Figure 15   Calculated battery temperatures for battery with half as many cells, showing effects of different thermal control options. PCM option is much lighter and smaller that conventional design. (Heat power shown for 200 W case.)

41

5.3   LEO Surge Mode Simulation

LEO surge mode - LEO applications requiring high heat dissipation over a short time present difficult thermal control problems. Examples of high rate LEO discharge are:

- SPACE-BASED RADAR - SBR is expected to have a surge power lasting about 9 minutes.
- IRIDIUM - The high traffic associated with passage of the LEO satellite over a population center is expected to cause a high rate of battery use lasting a few minutes
- BURST POWER - Military weapons applications may call for surge power lasting on the order of minutes

We consider a dissipation profile having $10x$ higher power for a $10x$ shorter duration than the GEO case. The temperature response of the Eagle Picher RNH-78 cell with and without PCM capacity enhancement was calculated with the two-node model and the results are shown in Figure 21. Additional PCM heat capacity reduces the temperature rise roughly in direct proportion to the heat capacity. In order to be as effective as shown, it is required that the PCM be thermally well coupled to the cells, and PCC design is meant to serve that requirement.

Burst Power in LEO
Battery temperature response

Legend
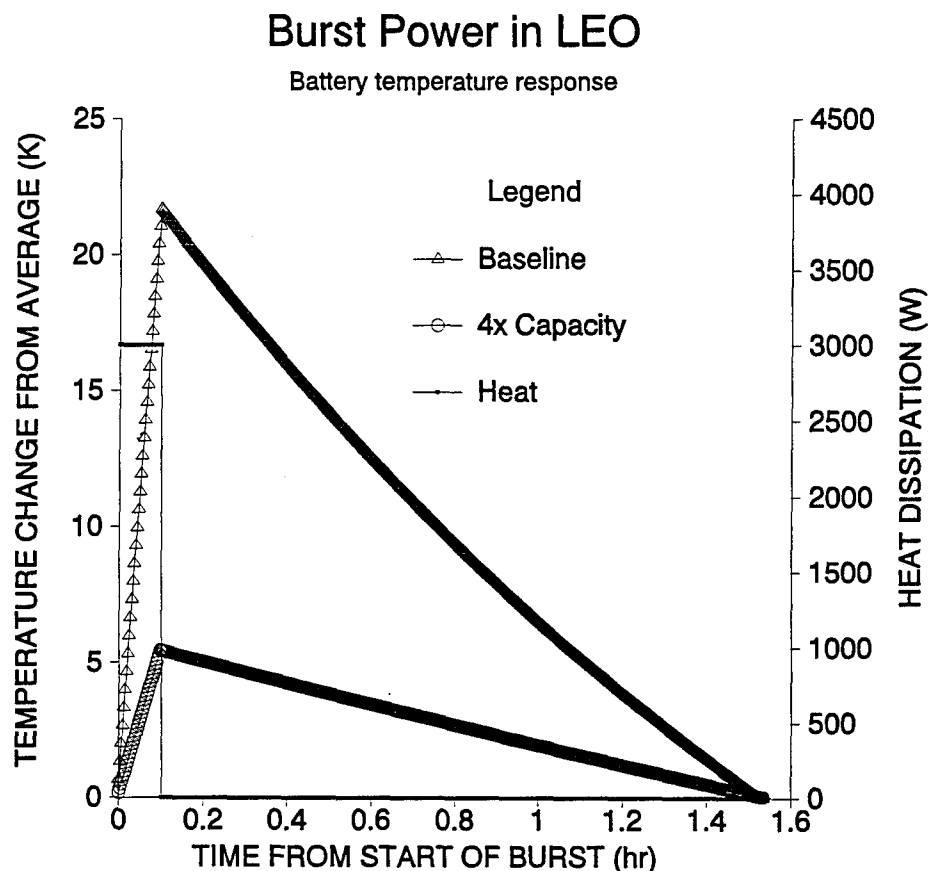- △ Baseline
- ○ 4x Capacity
- —— Heat

Figure 16   Numerical simulation of LEO high power surge lasting 0.11 hr. Peak temperatures decrease in proportion to the capacity increase.

<u>Effects neglected</u> - The two-node model has ignored certain effects that may be included by adding other nodes and coupling features:

- cell internal gas gap resistance (add one node, one capacity, one resistance)
- battery sleeve thermal resistance (add one node, one resistance)
- baseplate resistance and capacity (add one node, one resistance, one capacity)

The two-node model is useful and has allowed a significant analysis to be performed with a simple spreadsheet program suited to Phase 1 study purposes. When these other effects are included, it is perhaps preferable to then use a packaged thermal modeling program with at least 3-D axisymmetric capabilities.

5.4 Multinode Sleeve Model

When configured with adequate volume and latent heat, the phase-change sleeve will absorb, store and release heat at a relatively constant temperature compared with the aluminum sleeves. To begin investigating this behavior in detail, a simple cell and sleeve configuration was studied numerically with a Fortran forward difference code that permitted tens to hundreds of nodes to run quickly on a microcomputer.

The configuration of cell and sleeve considered is shown in Figure 22. Cell diameter is 8.9 cm (3.5") and cell height is 17.3 cm (6.8"). Hemispherical end caps are replaced by flat ends to render the problem axisymmetric and 2-D, without change in essential behavior. The end caps are assumed adiabatic and heat conducts through the cell volume to the sleeve, across the cell-sleeve interface, and then into and down the sleeve. For heat transfer coefficients greater than 100 W/K-m^2, the interface impedance is insignificant and is therefore neglected. The cell thermal conductivity is 2
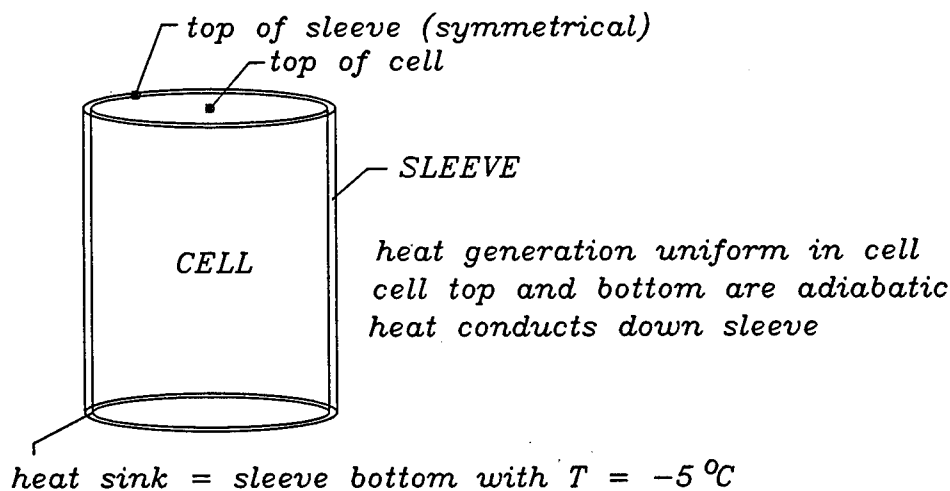

CALCULATE TEMPERATURES AT ...

Figure 17   Configuration of cell and sleeve for finite difference thermal calculation.

W/m-K (isotropic) and the cell heat capacity is 1.0 J/K-cm^3. The sleeve thickness assumed is 1 mm for the aluminum sleeve, with aluminum thermal conductivity 180 W/m-K, and 2.5 mm for the water portion of the PCC sleeve, with thermal conductivity = 0.6 W/m-K. The PCC sleeve thermal conductivity is assumed to be k = 30 W/m-K (isotropic) to account for the combined effect of radial carbon fibers in low density and a thin cylindrical aluminum liner 0.16 mm thick (0.006"). The temperatures are calculated over a 100-node grid, with 5 radial bands and 20 axial layers. The highest temperature during heating is at the top center of the cell. The lowest temperature is always at the sleeve bottom boundary condition of -5°C. Three temperatures are presented below: at the top of the cell, at the top of the sleeve, and the average temperature throughout the cell, excluding the sleeve.

Cell and sleeve temperatures for GEO eclipse - The results of the finite element calculation for heat dissipation of 10 W for 4000 s (corresponding to GEO equinox eclipse) are shown in Figures 23 and 24. The cell temperature in the PCC case is at all times closer to 0°C than in the aluminum case. The cell temperature is higher than the sleeve temperature because of the internal cell gradient. During the heating phase, the high-capacity PCC sleeve absorbs and stores heat, keeping cell temperatures lower than the aluminum sleeve, as desired. During the following cooling phase, the PCC sleeve stays warmer because of its stored heat. The long time scale of cooling is partly due to the lower thermal conductance of the PCC sleeve. At approximately 15000 s, the PCC sleeve freezes completely.

In satellite applications the heat sink temperature is well below -5°C and cell heaters are used when sleeve temperatures fall below a set point, typically at -3°C. The calculation performed here indicates that the PCC sleeve would require significantly less heating power than the aluminum case for two reasons: (1) the heat stored displaces heat required later and (2) the sleeve heat leak conductance is lower.

Cell and sleeve transient temperatures for LEO surge - The calculation was applied to a LEO power surge of 100 W lasting 400 s. The results of the calculation are shown in Figures 25 and 26. The cell temperature in the PCC case is at all times closer to 0°C than in the aluminum case. Compared to the above case with ten-times lower power lasting ten-times longer, this case has higher gradients between the cell and sleeve. Although the energy deposited is the same, the transient cell temperatures are significantly higher. In the aluminum sleeve case, the cell top temperature remains above 20°C for approximately 1000 s, but in the PCC case, temperature never exceeds 20°C.

Figure 18   GEO eclipse transient temperatures for the aluminum and the PCC sleeves. Parameters used are discussed in text.

Figure 19   Average GEO eclipse transient temperatures for the aluminum and the PCC sleeves.

45

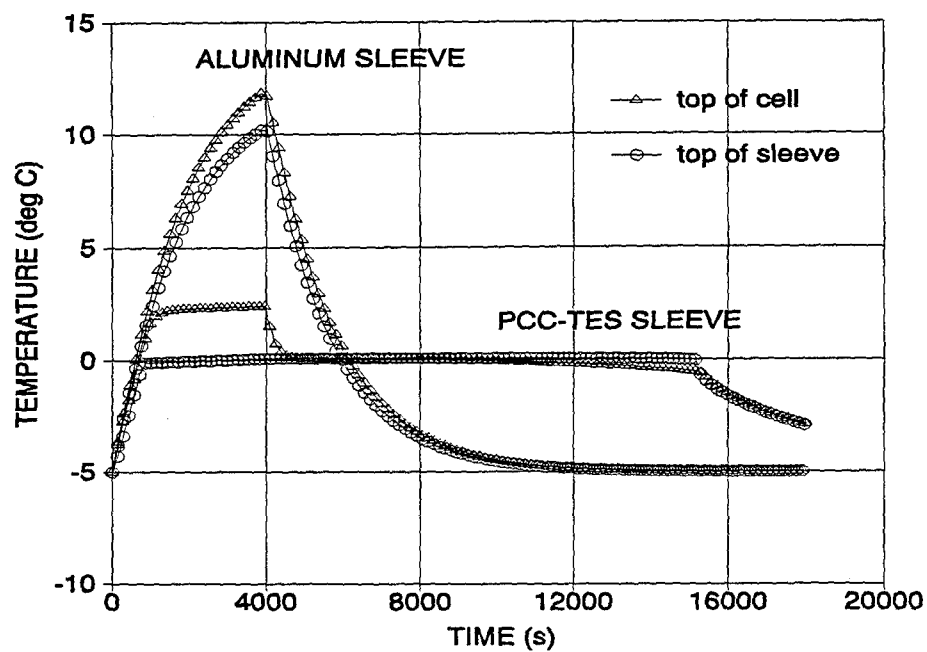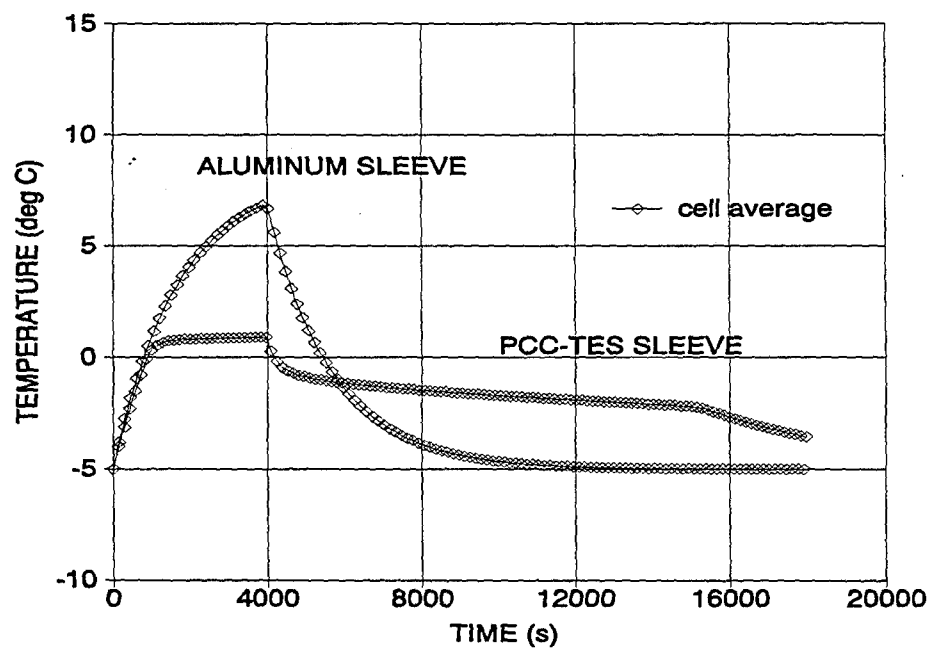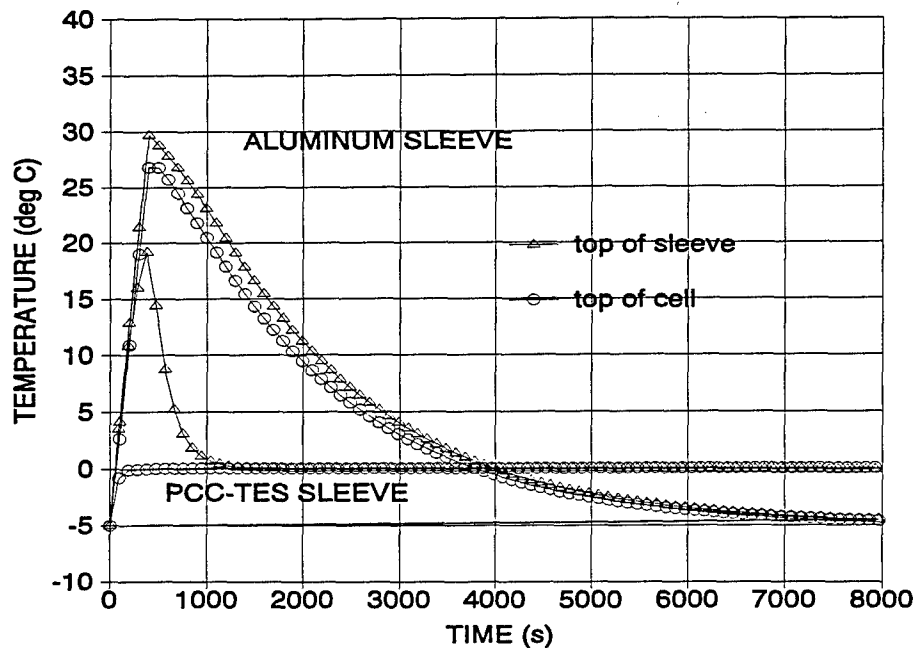**Figure 20**   LEO power surge mode transient temperatures for the aluminum and the PCC sleeves. Parameters used are discussed in text.
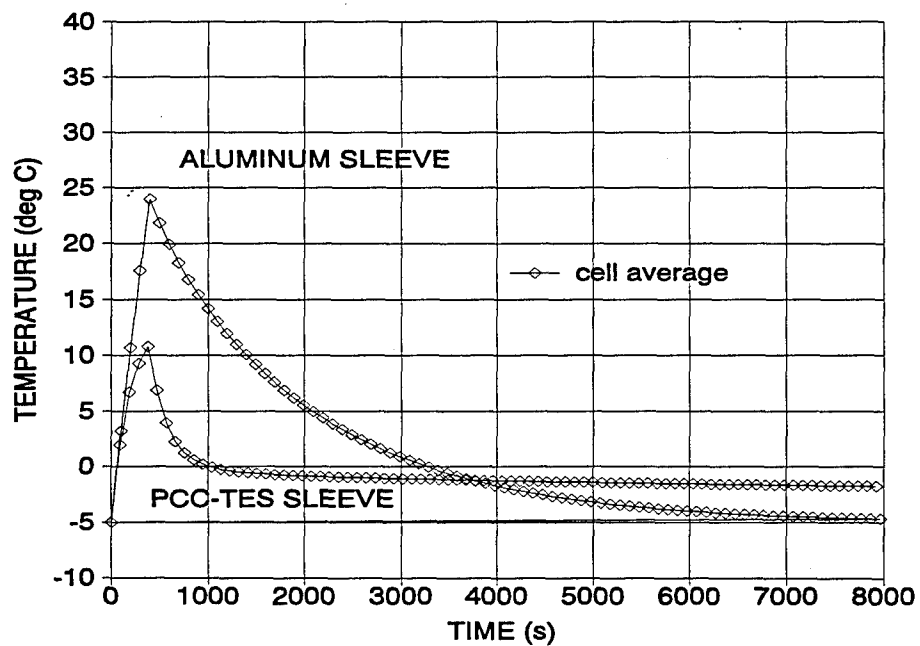

Figure 21   Average LEO power surge mode transient temperatures for the aluminum and the PCC sleeves.

Effects neglected - The above calculation is a preliminary analysis and has not included 3-D geometrical effects such as the cell internal structure, conduction anisotropy resulting from the layer structure of the cell elements, and gas volumes in domes at the ends of the cell. The temperatures throughout the cell at all phases of the orbit are of interest in optimizing sleeve design. Also, the actual heat sink should include thermal resistance to the radiator, radiator effectiveness, and applied heater power as required to maintain temperatures.

Sleeve thermal resistance - The thermal resistances of conventional aluminum and of PCC sleeves are shown in Table XII. The radial thermal resistance is very low compared to the axial thermal resistance, because of the geometry. This is relatively unimportant for the aluminum sleeve, where the concern is primarily to lower the axial thermal resistance and decrease the axial temperature gradient. For the PCC case the fact that the radial thermal resistance is low assures that the heat can be absorbed in the PCM matrix with a low temperature gradient. It is desirable that the axial thermal resistance of the PCC sleeve be higher than for conventional design, because that favors longer sleeve RC time constant and helps to hold transient heat in the cell and assure that a more constant, better averaged, heat dissipation is passed to the thermal control system.

The PCC metallic liner required is thinner than the conventional aluminum sleeve. For example, when the liner is half as thick, the axial thermal resistance is approximately twice as high. The RC time constant increases by roughly a factor of 10, because the C is increased by 5, and the R is increased by 2. The power dissipated reduces by a factor of 10 to the average value. The net effect on the sleeve temperature gradient is a reduction by a factor of 5. This analysis neglects the effect of heat conduction through the volume of the cell itself, which would further reduce the temperature gradient.

47

Table XI   The axial and radial thermal resistance of various sleeves.

Aluminum Sleeve:

full length =	17.3	cm
ID =	8.89	cm
thickness =	0.05	cm
end face area =	1.40	cm2
volume =	24.25	cm3
side face area =	482.4	cm2
thermal conductivity =	2.0	W/cm-K
axial thermal resistance =	3.07	K/W
radial thermal resistance =	0.000052	K/W

PCC-TES Sleeve:

full length =	17.3	cm
ID =	8.89	cm
thickness =	0.25	cm
end face area =	7.18	cm2
volume =	123.99	cm3
side face area =	482.4	cm2
axial thermal conductivity =	0.02	W/cm-K
radial thermal conductivity =	0.3	W/cm-K
axial thermal resistance =	60.15	K/W
axial with 0.5 mm Al =	2.92	K/W
radial thermal resistance =	0.001728	K/W

Thermal Resistance:	Axial	Radial	
1-mm aluminum =	1.53	0.000104	K/W
2.5-mm thick PCC =	60.15	0.002073	K/W
0.5-mm Al + 2.5 mm PCC =	2.92	0.001728	K/W

6   CONCLUSIONS

6.1   PCM Benefits

PCCs appear suited for Ni-H$_2$ space batteries applications because
- Ni-H$_2$ batteries they require tight temperature control ($\pm 5°C$) for good cycle life and
- they have low intrinsic heat capacity that calls for large radiators and large backup heater power

Water-based PCM sleeves can increase the effective battery heat capacity by 400% at 15% cost in battery weight, which is easily offset by savings in radiator size, PV heater power, and total battery plus thermal control system mass.

The net effect is improved battery temperature control (lower operating temperature, more temperature uniformity among the cells) and reduced system weight and power. The benefits of PCM thermal control increase with increasing battery DOD. PCM thermal control is an enabling technology for the reliable use of lightweight, high-DOD Ni-H$_2$ space batteries.

Benefits - The principal benefits of the PCMs in batteries are the following:
- reduced size and weight of the thermal control system
- reduced heating requirement with smaller radiators for GEO applications
- longer battery cycle life as a result of smaller temperature swings
- higher charge efficiency resulting from more uniform temperatures throughout the cell and between cells in a battery
- less need for diode heat pipes

Applications - The principal Ni-H$_2$ battery applications for PCM are the following:
- thermal control of deep-DOD battery uses
- retrofits in existing satellite designs originally intended for Ni-Cd batteries
- GEO communications and data relay satellites
- multicell CPV designs for both GEO and LEO missions
- LEO Space Based Radar
- LEO mobile telephone systems (IRIDIUM, GlobalStar)
- Mars Lander
- battery manpacks and SSF Modular Power Systems

Other battery applications for PCM are
- PCM-enhanced carbon-carbon sleeves for Na-S batteries
- Li batteries (eg NASA-JSC Battery Manpack for EVA)
- NiMH batteries (electric vehicles)

6.2 Stress Relief by Capillary Void Control

Phase 1 has demonstrated that electroflocked carbon fiber wick structures can provide the desired heat conductance and stress relief to allow freeze-melt cycling without fracture. It is a significant achievement that this has been demonstrated with water as the PCM, because water is notoriously risky to use in thermal energy storage applications. No prior spacecraft PCM study has seriously considered water as the PCM, presumably because of thermal stress problems. ESLI has demonstrated that the void distribution in water can be controlled to eliminate expansion stress caused when water freezes to ice.

The option of using water as PCM is important because water-based PCCs can be roughly half as large and half as heavy as PCM devices based on alternative organic PCMs. Water PCM is preferred for commercial applications because it poses less of a fire hazard and is readily available.

6.3 Phase 2 Recommendations

A Phase 2 program would provide initial qualification of PCC thermal control devices for Air Force spacecraft applications. Commercial satellite and electric vehicle applications should follow in Phase 3. Lightweight PCC device fabrication and operation would be demonstrated.

Phase 2 prototype Ni-H$_2$ battery sleeves should be developed. Initial thermal performance and cycle life testing of sleeves during freeze-melt cycling would be performed at ESLI. Phase 2 would culminate in the testing of a two or three cell battery that is thermally tested in vacuum. The effects to be observed in thermal vacuum testing are the temperature excursions at various locations on the battery and the amount of heater power required to maintain minimum temperature. A control battery with conventional sleeve design would be tested for control purposes. Generic plate and box PCM heat sink configurations should also be developed, based on ESLI PCC design with electroflocked carbon fiber wick structures. These could serve as PCC baseplates for batteries or electronics devices in spacecraft and terrestrial applications.

6.4 Phase 3 Possibilities

Qualification of PCC technology will be necessary for use in commercial satellites. A successful Phase 2 would be a major step in positioning PCC technology for a space qualification program. Phase 3 ideally would involve a flight experiment in which a PCC thermal control component would be used with a Ni-H$_2$ battery.

Commercial potential - All commercial satellites use batteries, and there is significant potential for the proposed PCC thermal control component to increase the reliability and reduce the costs of space battery subsystems. New programs are pushing for higher DOD and lighter batteries,

both of which aggravate thermal control. The commercial market is very competitive and margins will be cut, creating opportunities for innovative lightweight thermal control options.

PCC thermal control technology is potentially useful in a broad range of transient thermal control situations, including

- periodic thermal loading from electronic and environmental sources
- surge power thermal control
- thermal bus load management in multimodule space platforms, where stochastic demand causes fluctuating loads
- load management of terrestrial pulsed power and high power electrical switching equipment

BIBLIOGRAPHY

Betz, F; J F Stockel, and A Gaudet; "Nickel-Hydrogen Storage Battery for use on Navigation Technology Satellite-2," 11th IECEC (1976) Vol. 1, pp. 510-516

Dunlop, J D; "Nickel-Hydrogen Batteries," in *Handbook of Batteries and Fuel Cells*, David Linden, ed., McGraw-Hill, NY, 1984, pp. 22.1-22.17.

Kerr, R.L.; "Heat Generation in Nickel-Hydrogen Cells," 21st IECEC Paper 86-9344 (1986) pp. 1521-1526

Kim, Junbom; T V Nguyen; R E White; "Thermal Mathematical Modeling of a Multicell Common Pressure Vessel Nickel-Hydrogen Battery," J Electrochem Soc 139 (1992) p 2781-2787

Knowles, T.R. and Webb, G.W.; "Metal/Phase-Change Material Composite Heatsinks" Air Force SBIR Contract No. F33615-84-C-3417 Final Report, AFWAL-TR-88-3069, October 1988.

Landolt-Börnstein, 4. Band, 6. Auflage, 1961 (Springer Verlag)

Ryu, Si-Ok; DeWitt, K J; Keith, T G; "Thermal Modeling of a Ni-H$_2$ Battery Cell," Final Report NASA Grant NCC 3-69, NTIS No. N91-25319, 1991

Scott, W.R.; "Heat Rate and Coulombic Efficiency of Nickel-Hydrogen Battery Cells During Simulated Geosynchronous Orbit Cycling," 18th IECEC Paper 839237, 1983, pp. 1453-1459.

DISTRIBUTION LIST

AUL/LSE
Bldg 1405 - 600 Chennault Circle
Maxwell AFB, AL 36112-6424   1 cy

DTIC/OCP
8725 John J. Kingman Rd Ste 944
FT Belvoir, VA 22060-6218   2 cys

AFSAA/SAI
1580 Air Force Pentagon
Washington, DC 20330-1580   1 cy

PL/SUL
Kirtland AFB, NM 87117-5776   2 cys

PL/HO
Kirtland AFB, NM 87117-5776   1 cy

Official Record Copy

PL/VTP/Larry Crawford   2 cys

Dr. R. V. Wick   1 cy
PL/VT
Kirtland, AFB, NM 87117-5776